University of Stuttgart
Institut of Geodesy

Gravity Inversion
Using Point Mass Distribution

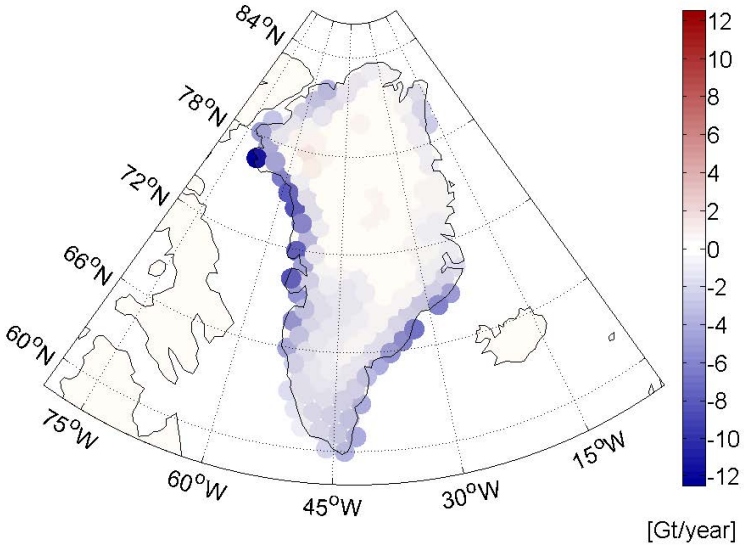

Master Thesis
in study program GEOENGINE
University of Stuttgart

Yuchen Han

Stuttgart, June 2017

Supervisor: Prof. Dr.-Ing. Nico Sneeuw
Dipl.-Ing. Matthias Roth

Declaration

I declare that this thesis has been composed solely by myself and that it has not been submitted, in whole or in part, in any previous application for a degree. Except where stated otherwise by reference or acknowledgement, the work presented is entirely my own.

Place, Date Signature

Abstract

Global climate change is a serious problem influencing our environment and Greenland ice mass loss is one of the phenomena of climate change. Every year hundreds of gigaton of ice melts and flows into the ocean, which causes the rising of the global sea level. This work is to estimate the ice mass loss of Greenland with the gravitational signals derived from GRACE (Gravity Recovery And Climate Experiment) data. The point-mass modelling applied in this work enables us to infer the mass variations on the Earth's surface from the gravitational signals at satellite altitude. In order to solve the derived observation equations and stabilize the ill-posed problem, we apply the least-squares adjustment with Tikhonov regularization. Our simulation studies and real data experiment show that point-mass modelling provides both rational mass variation results and high-resolution spatial mass variation patterns. The numerical results indicate that on average near 300 km^3 of ice melts and flows into the ocean from Greenland every year.

Key words: GRACE, Mass variation, gravity inversion, Least-squares adjustment, Tikhonov regularization, L-curve criterion

Contents

1 Introduction **1**
1.1 Motivation . . . 1
1.2 Theory and methodology . . . 1
1.3 Outline of this work . . . 2

2 Data **3**
2.1 Data source . . . 3
2.2 Data processing . . . 3

3 Point-mass modelling methodology **7**
3.1 Point-mass modelling for one terrestrial mass point . . . 7
3.2 Point-mass modelling for a set of terrestrial mass points . . . 8

4 Regularization solution **11**
4.1 Gauss-Markov model . . . 11
4.2 Tikhonov regularization . . . 11
4.3 L-curve criterion . . . 12

5 Simulation Studies **15**
5.1 Area determination . . . 15
5.2 Determination of the distribution density for terrestrial mass points and space locations . . . 17
5.3 Noise-free simulation . . . 18
5.3.1 Noise-free simulation for low mass point distribution density . . . 19
5.3.2 Noise-free simulation for high mass point distribution density . . . 23
5.4 Simulation with noise . . . 27
5.4.1 Simulation with noise for low mass point distribution density . . . 27
5.4.2 Simulation with noise for high mass point distribution density . . . 31
5.5 The conclusion of the simulation studies . . . 35

6 Experiment using real GRACE data **37**
6.1 Determination of terrestrial mass points and space locations . . . 37
6.2 The gravity inversion process . . . 39
6.3 The gravity inversion result . . . 41

7 Conclusion **47**

List of Figures

2.1 The position of space location S at satellite altitude 5
2.2 GRACE-derived monthly gravitational deviations for space location S at satellite altitude 5

3.1 Point-mass modelling geometry 7
3.2 The gravitational attraction between space locations and terrestrial mass points . 8

4.1 The generic form of the L-curve (Hansen, P.C., 2008) 12
4.2 The L-curve for the small example 13

5.1 The chosen area over Greenland (Google, 2017) 16
5.2 The gravitational deviations at satellite altitude (500 km) caused by one point-mass variation (dm=-5 Gt) 16
5.3 The projection on the Earth's surface of the chosen area for simulated observations at satellite altitude (Google, 2017) 17
5.4 level 5-8 of point distribution density 18
5.5 The distribution of the defined mass points over Greenland (80) and the space locations at satellite altitude of simulated observations (464) 19
5.6 The defined point-mass variations on the Earth's surface (62) and the corresponding gravitational signals at satellite altitude (464) 19
5.7 The ordinary least-squares solution of the noise-free simulation for low mass point distribution density 20
5.8 The graph plotting the solution norm against residual norm of the noise-free simulation for low mass point distribution density 21
5.9 The Tikhonov-regularized least-squares solutions of the noise-free simulation for low mass point distribution density 22
5.10 The distribution of the defined mass points over Greenland (256) and the space locations at satellite altitude of simulated observations (464) 23
5.11 The defined point-mass variations on the Earth's surface (128) and the corresponding gravitational signals at satellite altitude (464) 23
5.12 The ordinary least-squares solution of the noise-free simulation for high mass point distribution density 24
5.13 The graph plotting the solution norm against residual norm of the noise-free simulation for high mass point distribution density 25
5.14 The Tikhonov-regularized least-squares solutions of the noise-free simulation for high mass point distribution density 26
5.15 The defined point-mass variations on the Earth's surface (62) and the corresponding gravitational signals including noise at satellite altitude (464) 27
5.16 The ordinary least-squares solution of the simulation with noise for low mass point distribution density 28

5.17 The graph plotting the solution norm against residual norm of the simulation with noise for low mass point distribution density 28
5.18 The Tikhonov-regularized least-squares solutions of the simulation with noise for low mass point distribution density 30
5.19 The defined point-mass variations on the Earth's surface (128) and the corresponding gravitational signals including noise at satellite altitude (464) 31
5.20 The ordinary least-squares solution of the simulation with noise for high mass point distribution density 31
5.21 The graph plotting the solution norm against residual norm of the simulation with noise for high mass point distribution density 32
5.22 The Tikhonov-regularized least-squares solutions of the simulation with noise for high mass point distribution density 34

6.1 The determination of terrestrial mass points (196) and space locations (353) for the Gravity inversion 38
6.2 The observation vectors containing GRACE-derived monthly gravitational deviations 39
6.3 The observation equations and the solutions containing monthly mass deviations 40
6.4 The L-curve of the gravity inversion process, exemplary for the month May 2004 41
6.5 The monthly total mass deviations and the linear regression result 42
6.6 The positions of terrestrial mass point P_9 and P_{184} on Greenland 42
6.7 The monthly mass deviations and the linear regression result at terrestrial mass point P_9 43
6.8 The monthly mass deviations and the linear regression result at terrestrial mass point P_{184} 43
6.9 The distribution of the mass variations on Greenland 44
6.10 The positions of terrestrial mass point P_{55} and P_{59} on Greenland 45

List of Tables

5.1 The summary of the noise-free simulation for low mass point distribution density 21
5.2 The summary of the noise-free simulation for high mass point distribution density 25
5.3 The summary of the simulation with noise for low mass point distribution density 29
5.4 The summary of the simulation with noise for high mass point distribution density 32

Chapter 1

Introduction

1.1 Motivation

Climate change is a serious environment problem for human beings and Greenland ice mass loss is one of the phenomena of this problem. According to research, hundreds of gigaton of ice melts and flows into the ocean every year, which leads to the rising of the global sea level. In order to estimate the ice mass loss in Greenland, some direct and indirect methods are applied for this purpose. For instance, some researchers measure the thickness change of the ice with the help of sonar system and estimate the ice mass loss in volume. Others indirectly measure the gravity change locally with gravimeters to estimate the mass change at the location (Hurt, P., 2015). Most of these methods have the disadvantage that they need much manpower and material resource.

However, the GRACE (Gravity Recovery And Climate Experiment) satellite mission provides us a convenient alternative method to estimate large scale mass variations on the Earth's surface. The GRACE satellite mission has been providing time-variable gravity field information from space since it was launched in 2002. Using the gravity data from GRACE, we can calculate the gravity changes at satellite altitude in a specific time sequence and from these gravitational signals we can perform the gravity inversion to derive the estimation of the mass variations in the area of interest on the Earth's surface.

1.2 Theory and methodology

Since we want to estimate the Greenland ice mass loss from the GRACE data, we need to relate the gravitational signals at satellite altitude in space and the mass variations on the Earth's surface. The point-mass modelling methodology can relate these two sides of the inversion and yield the observation equations between both sides. The basic idea behind point-mass modelling is to attribute mass variation to individual surface locations and build up the geometrical relationship between the surface locations and the space locations at satellite altitude. The surface locations attributed with mass variations are called mass points in this thesis.

If we want high-resolution spatial mass variation patterns of the studied area, we need to distribute the mass points at a high density. However, in this case the determination of surface mass variations from the gravitational signals in space can become ill-posed, i.e., the design matrix of the derived observation equation is near rank-deficient. In such cases the

ordinary least-squares solution, derived with Gauss-Markov model, is unstable. Here we need Tikhonov regularization to stabilize the solution. The key to Tikhonov regularization is to find the proper regularization parameter and calculate the corresponding Tikhonov regularized least-squares solution, which is considered to be the optimal solution. There are several approaches to find the proper regularization parameter and in this work we apply the L-curve criterion since it has been shown to provide good results when compared with other strategies (Baur, O. and Sneeuw, N., 2011).

1.3 Outline of this work

This thesis is structured as follows. Chapter 2 introduces the data provided by GRACE and explains the process of deriving the observations from GRACE data for the gravity inversion. Chapter 3 introduces the point-mass modelling methodology. It illustrates how to build up the geometrical relationship between the surface mass points and the space locations at satellite altitude and derive the design matrix of the observation equations of the gravity inversion. Chapter 4 demonstrates the theory of Tikhonov regularization and the L-curve criterion used in this work. In chapter 5, a series of closed-loop simulation studies are conducted to figure out in which cases Tikhonov regularization is necessary and to evaluate the L-curve criterion. In Chapter 6, we perform the gravity inversion with GRACE-derived observations and obtain the results according to the conclusion drawn from the simulation studies in Chapter 5. Chapter 7 represents the conclusion of this whole work.

Chapter 2

Data

The data in this work is derived from the GRACE (Gravity Recovery And Climate Experiment) satellite mission, which is launched in March 2002. GRACE consists of two identical spacecraft that fly about 220 km apart in a polar orbit 500 km above the Earth. GRACE maps Earth's gravity field by making accurate measurements of the distance between the two satellites, using GPS and a microwave ranging system (NASA, 2012).

2.1 Data source

Since 2002, the GRACE satellite mission has been providing time-variable gravity field solutions, which are typically released to the public in terms of fully normalized spherical harmonic coefficients $\bar{c}_{lm}$ and $\bar{s}_{lm}$ of the Earth's external gravitational potential. There are several institutes releasing the data to the public, such as JPL (Jet Propulsion Laboratory, California Institute of Technology), CSR (Center for Space Research, the University of Texas at Austin) and GFZ (Helmholtz-Zentrum Potsdam Deutsches GeoForschungsZentrum). For our work we used the latest release (RL05.1) GRACE-only gravity field estimates provided by JPL. In order to prevent aliasing effects of strong seasonal signals from falsifying the time-series analysis, we chose the total time span of the gravity field series to cover an integer number of years. According to available monthly GRACE solutions from the data, we investigate a 14-year sequence from April 2002 to March 2016.

2.2 Data processing

The data we used provide us fully normalized spherical harmonic coefficients ($\bar{c}_{lm}$, $\bar{s}_{lm}$) and their standard deviations ($\sigma_{\bar{c}_{lm}}$, $\sigma_{\bar{s}_{lm}}$). The maximum spherical harmonic degree is 90 while in our work we read the data until degree-60 for our calculation. Since the main purpose of this thesis is to infer the mass variations on the Earth's surface from gravitational signals at satellite altitude, we first need to derive the gravitational deviations from the GRACE data for the inversion and the process is illustrated in this section.
Residual spherical harmonic coefficients according to

$$d\bar{c}_{lm} = \bar{c}_{lm} - \bar{c}_{lm}^{\text{mean}} \quad \text{and} \quad d\bar{s}_{lm} = \bar{s}_{lm} - \bar{s}_{lm}^{\text{mean}} \tag{2.1}$$

represent deviations of a monthly gravity field from a temporal mean. In Equation (2.1), $\bar{c}_{lm}^{\text{mean}}$ and $\bar{s}_{lm}^{\text{mean}}$ indicate static mean values of the 14-year sequence. From this we can compute the monthly gravitational deviations from the temporal mean in the 14-year sequence with

$$dg = -\frac{GM}{r^2}\sum_{l=2}^{L}(l+1)\left(\frac{a}{r}\right)^l\sum_{n=0}^{l}\bar{P}_{lm}(\sin\varphi)[d\bar{c}_{lm}\cos m\lambda + d\bar{s}_{lm}\sin m\lambda] \tag{2.2}$$

(Baur, O. and Sneeuw, N., 2011). Therein $(\lambda,\ \varphi,\ r)$ denote spherical polar coordinates with λ longitude, φ latitude and r distance from the geocenter. GM is the geocentric constant, a indicates the semi-major axis of a reference ellipsoid of revolution ($a = 6378.1363$ km). $L = l_{\max}$ is the maximum spherical harmonic degree and in this study $L = 60$. Degree-0 and degree-1 coefficients cannot be resolved reliably from GRACE and hence were neglected. The latitude-dependent functions $\bar{P}_{lm}(\sin\varphi)$ represent the 4π-normalized associated Legendre functions.

GRACE is unable to separate the direct disturbance from the deformation-induced indirect disturbance. Therefore, Equation (2.2) accounts for both effects, which means that the deformation potential is misinterpreted as signal counteracting the deglaciation signal. Indeed, the spherical harmonic coefficients on the right-hand side of Equation (2.2) can be represented as $d\bar{c}_{lm} = d\bar{c}_{lm}^{\text{mass}} + k_l d\bar{c}_{lm}^{\text{mass}}$ and $d\bar{s}_{lm} = d\bar{s}_{lm}^{\text{mass}} + k_l d\bar{s}_{lm}^{\text{mass}}$, where the first terms $(d\bar{c}_{lm}^{\text{mass}},\ d\bar{s}_{lm}^{\text{mass}})$ indicate the contribution of mass-redistribution and the second terms $(k_l d\bar{c}_{lm}^{\text{mass}},\ k_l d\bar{s}_{lm}^{\text{mass}})$ are the contribution of the Earth's deformation; k_l denote the degree-dependent load Love numbers (Baur, O. and Sneeuw, N., 2011). Besides, we need to consider that the direction of $\boldsymbol{r}$ is pointing outwards, which is opposite to the direction of gravitational acceleration. Hence, multiplying Equation (2.2) by -1 and isolating the mass re-distribution effect yield

$$dg^{\text{mass}} = \frac{GM}{r^2}\sum_{l=2}^{L}\frac{(l+1)}{(1+k_l)}\left(\frac{a}{r}\right)^l\sum_{n=0}^{l}\bar{P}_{lm}(\sin\varphi)[d\bar{c}_{lm}\cos m\lambda + d\bar{s}_{lm}\sin m\lambda]. \tag{2.3}$$

For the sake of simplified notation, in the following we omit the term "mass".

Using Equation (2.3) we can calculate the monthly gravitational deviations from the temporal mean for any space location at satellite altitude. Figure 2.1 and 2.2 illustrate the calculation as an example for space location S at satellite altitude with spherical polar coordinates $(\lambda,\ \varphi,\ r)$. Figure 2.1 displays the position at satellite altitude of space location S; figure 2.2 indicates the monthly gravitational deviations dg in the 14-year sequence at space location S and the corresponding linear regression result. Like in this example, we can calculate the monthly gravitational deviations for all the space locations at satellite altitude, which are selected for our studies, and these GRACE-derived monthly gravitational deviations are just the observations for the gravity inversion in Chapter 6.

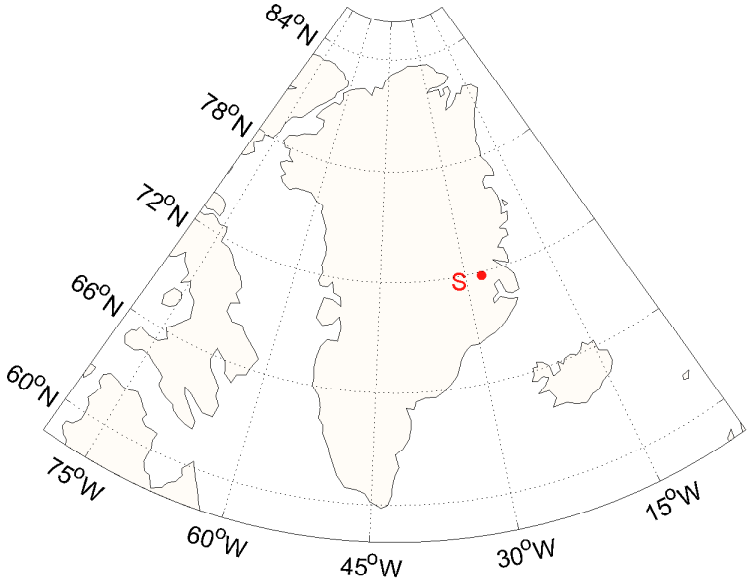

Figure 2.1: *The position of space location S at satellite altitude*

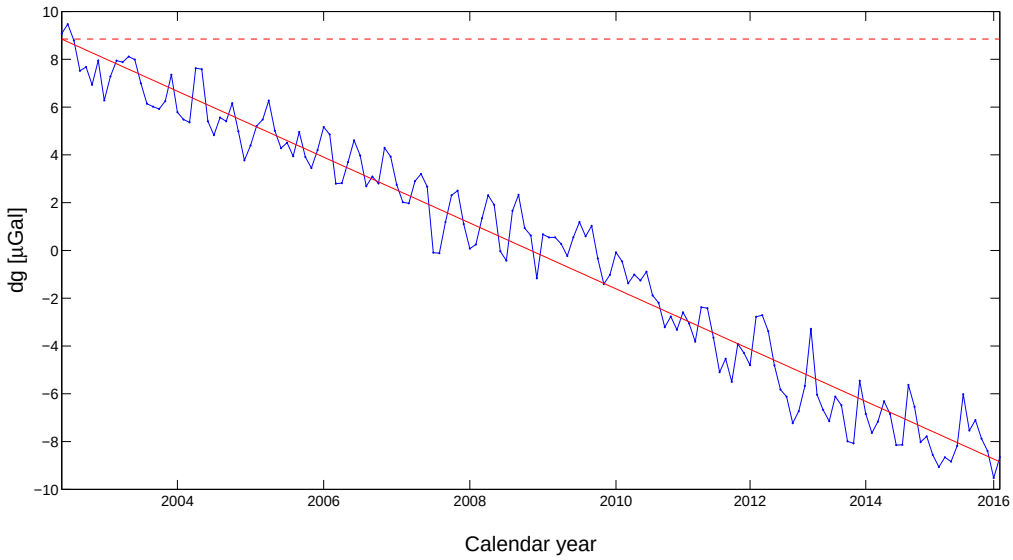

Figure 2.2: *GRACE-derived monthly gravitational deviations for space location S at satellite altitude*

Chapter 3

Point-mass modelling methodology

This chapter introduces the point-mass modelling methodology, which relates the gravitational signals at satellite altitude and the mass variations attributed to individual terrestrial mass points on the Earth's surface. With this methodology we can derive the observation equations for our following studies.

3.1 Point-mass modelling for one terrestrial mass point

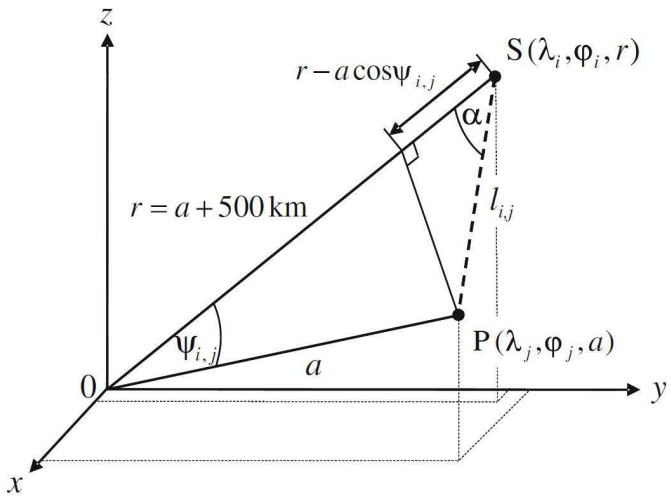

Figure 3.1: *Point-mass modelling geometry*

Point-mass modelling relates gravitational deviations in space $dg_i (i = 1, ..., s)$, such as derived from GRACE with Equation (2.3), to individual point-mass variations $dm_j (j = 1, ..., p)$ on the Earth's surface. According to Figure 3.1, the space location $\mathrm{S}(\lambda_i, \phi_i, r_i)$ and the terrestrial mass point $\mathrm{P}(\lambda_j, \phi_j, r_j)$ are separated by the spherical distance $\psi_{i,j}$ subject to

$$\cos\psi_{i,j} = \sin\phi_i \sin\phi_j + \cos\phi_i \cos\phi_j \cos(\lambda_i - \lambda_j). \tag{3.1}$$

Furthermore, the gravitational attraction between S and P along the distance $l_{i,j}$ separating them is $Gdm_j/l_{i,j}^2$. Hence, the radial attraction between the geocenter and the space location

becomes

$$dg_{i,j} = \frac{Gdm_j}{l_{i,j}^2}\cos\alpha = Gdm_j\frac{r_i - a\cos\psi_{i,j}}{l_{i,j}^3}. \tag{3.2}$$

The indices i and j emphasize that Equation (3.2) describes the gravitational attraction in S caused by an individual mass variation in P. Inserting $l = \sqrt{(a^2 + r_i^2 - 2ar_i\cos\psi_{i,j})}$ into Equation (3.2) finally leads to

$$dg_{i,j} = Gdm_j\frac{r_i - a\cos\psi_{i,j}}{(a^2 + r_i^2 - 2ar_i\cos\psi_{i,j})^{3/2}}. \tag{3.3}$$

3.2 Point-mass modelling for a set of terrestrial mass points

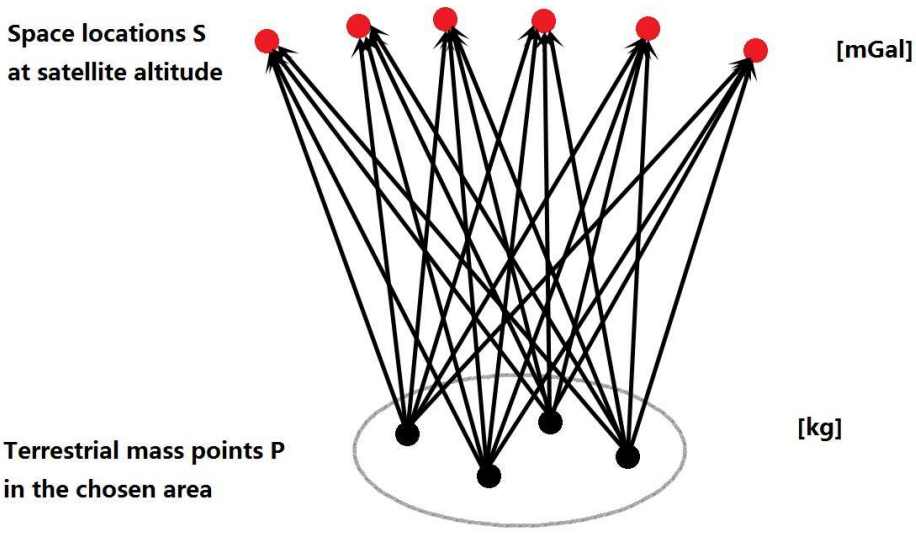

Figure 3.2: *The gravitational attraction between space locations and terrestrial mass points*

However, when our study is based on a set of mass points in a certain area on the Earth's surface, the gravitational attraction at one space location S is caused by the whole set of point-mass variations. As is shown in Figure 3.2, if we define a set of mass points and a corresponding set of space locations, the total gravitational deviation at each space location is caused by all the point-mass variations of the defined mass point set. Consequently, the total gravitational deviation in a defined set of space locations due to the full set of point-mass variations becomes

$$dg_{i,j} = G\sum_{j=1}^{p} dm_j\frac{r_i - a\cos\psi_{i,j}}{(a^2 + r_i^2 - 2ar_i\cos\psi_{i,j})^{3/2}},\ i = 1, ..., s. \tag{3.4}$$

Equation (3.4), together with the pseudo-observations derived with Equation (2.3), represents the functional model for the point-mass modelling approach. The left-hand side indicates GRACE-derived gravitational deviations. The right-hand side contains the unknown point-mass variations dm_j. Since our analysis is based on observations at satellite altitude, we ap-

point the geocenter distance for space locations to $r_i = r = a + 500$ km with an Earth radius $a = 6378.1363$ km.

Reformulation of the linear functional model in matrix-vector notation yields

$$\mathbf{y} = \mathbf{A}\mathbf{x} + \mathbf{e} \tag{3.5}$$

with the vector of observations $\mathbf{y}(s \times 1)$, the vector of unknown parameters $\mathbf{x}(p \times 1)$ and the design matrix $\mathbf{A}(s \times p)$. Its ith row and jth column element is

$$\mathbf{A}(i,j) = G\frac{(r_i - a\cos\psi_{i,j})}{(a^2 + r_i^2 - 2ar_i\cos\psi_{i,j})^{3/2}},\ i = 1,...,s,\ j = 1,...,p. \tag{3.6}$$

In addition, Equation (3.5) accounts for the case $s > p$, hence representing an overdetermined, inconsistent system of equations. The vector of residuals is denoted as $\mathbf{e}(s \times 1)$ (Baur, O. and Sneeuw, N., 2011).

Chapter 4

Regularization solution

This section explains the reason why we need regularization to solve the observation equation (Equation (3.5)) and introduces the parameter estimation methodology for Tikhonov regularization.

4.1 Gauss-Markov model

Generally, we can apply Gauss-Markov model to solve the linear equations in order to get best-unbiased estimates, whose observation equation is

$$\mathbf{y} = \mathbf{A}\mathbf{x} + \mathbf{e}. \tag{4.1}$$

The target function of this equation is

$$\mathcal{L}_A(\mathbf{x}) = \mathbf{e}^{\mathrm{T}}\mathbf{P}\mathbf{e} = (\mathbf{y} - \mathbf{A}\mathbf{x})^{\mathrm{T}}\mathbf{P}(\mathbf{y} - \mathbf{A}\mathbf{x}) = \min. \tag{4.2}$$

The minimization of the target function leads to the least-squares solution of the equation:

$$\hat{\mathbf{x}} = (\mathbf{A}^{\mathrm{T}}\mathbf{P}\mathbf{A})^{-1}\mathbf{A}^{\mathrm{T}}\mathbf{P}\mathbf{y}. \tag{4.3}$$

4.2 Tikhonov regularization

However, the upward continuation of the calculation with Equation (2.3) is a smoother and it can make the gravity inversion an ill-posed problem. Besides, when the mass points on the Earth's surface are very close to each other, the columns in design matrix $\mathbf{A}$ will become very similar, which makes the design matrix near rank-deficient and the normal equations matrix $\mathbf{N} = \mathbf{A}^{\mathrm{T}}\mathbf{P}\mathbf{A}$ become singular. In this case, the determination of surface mass changes from observations in space becomes ill-posed and the ordinary least-squares solution is unstable. Therefore, Tikhonov regularization is applied to stabilize the solution. Its target function is expressed as

$$\mathcal{L}_R(\mathbf{x}) = (\mathbf{y} - \mathbf{A}\mathbf{x})^{\mathrm{T}}\mathbf{P}(\mathbf{y} - \mathbf{A}\mathbf{x}) + \lambda\mathbf{x}^{\mathrm{T}}\mathbf{R}\mathbf{x} = \min, \tag{4.4}$$

where λ is the Lagrange multiplier of the constrained minimization problem, usually denoted as regularization parameter; $\mathbf{R}$ is the regularization matrix and here we take $\mathbf{R}$ as an identity

matrix **I**. Then the Tikhonov-regularized least-squares solution of Equation (4.1) becomes (Chen, T. et al., 2016)

$$\hat{\mathbf{x}} = (\mathbf{A}^{\mathrm{T}}\mathbf{P}\mathbf{A} + \lambda\mathbf{I})^{-1}\mathbf{A}^{\mathrm{T}}\mathbf{P}\mathbf{y}. \tag{4.5}$$

4.3 L-curve criterion

The appropriate choice of the regularization parameter λ is of crucial significance for the proper weighting of the penalty term against the residual norm. Unfortunately, neither is it known a priori nor does a straightforward analytical evaluation method exist. However, a variety of heuristic approaches have been proposed for the determination of the optimal regularization parameter λ_{opt} among a set of pre-defined values $\lambda_k, k = 1, ..., k_{max}$ (Baur, O. and Sneeuw, N., 2011). Here, we applied the L-curve criterion to acquire λ_{opt}. The criterion takes advantage of the typically L-shaped graph plotting the regularized solution norm $\|\hat{\mathbf{x}}_{\lambda_k}\|_2$ against the corresponding residual norm $\|\mathbf{y} - \mathbf{A}\hat{\mathbf{x}}_{\lambda_k}\|_2$ in log-log scale. In this way, the L-curve clearly displays the compromise between minimization of these two quantities, which is the heart of any regularization method (Hansen, P.C., 2008). The optimal regularization parameter is defined as the "corner" of the L-curve, i.e., the value that provides an estimate $\hat{\mathbf{x}}_{\lambda_k}$ with a good balance between the solution norm and residual norm.

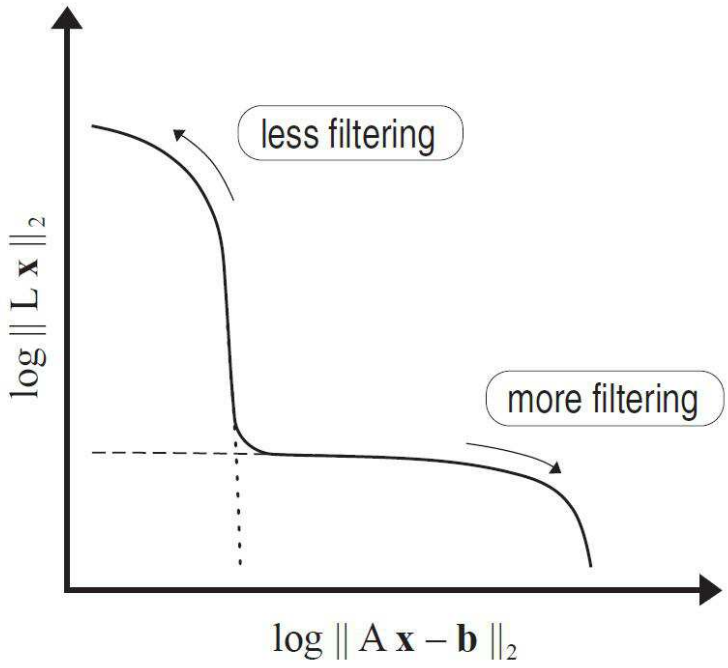

Figure 4.1: *The generic form of the L-curve (Hansen, P.C., 2008)*

Then we can use a small numerical example to demonstrate how L-curve criterion works. Assume that we have an observation equation $\mathbf{y} = \mathbf{A}\mathbf{x} + \mathbf{e}$ with the design matrix **A** and the

vector of observations $\mathbf{y}$ given by

$$\mathbf{A} = \begin{pmatrix} 0.16 & 0.10 \\ 0.17 & 0.11 \\ 2.02 & 1.28 \end{pmatrix} \qquad \mathbf{y} = \begin{pmatrix} 0.27 \\ 0.25 \\ 3.32 \end{pmatrix}$$

Here, the vector of observations $\mathbf{y}$ is generated by adding small errors to the exact observations corresponding to the exact solution $\bar{\mathbf{x}}^{\mathrm{T}} = (1\ 1)$:

$$\mathbf{y} = \begin{pmatrix} 0.16 & 0.10 \\ 0.17 & 0.11 \\ 2.02 & 1.28 \end{pmatrix} \begin{pmatrix} 1.00 \\ 1.00 \end{pmatrix} + \begin{pmatrix} 0.01 \\ -0.03 \\ 0.02 \end{pmatrix}$$

Firstly, we can compute the ordinary least-squares solution $\hat{\mathbf{x}}_{\mathrm{LSQ}}$ by Gauss-Markov model:

$$\hat{\mathbf{x}}_{\mathrm{LSQ}} = \begin{pmatrix} 8.47 \\ -10.78 \end{pmatrix}$$

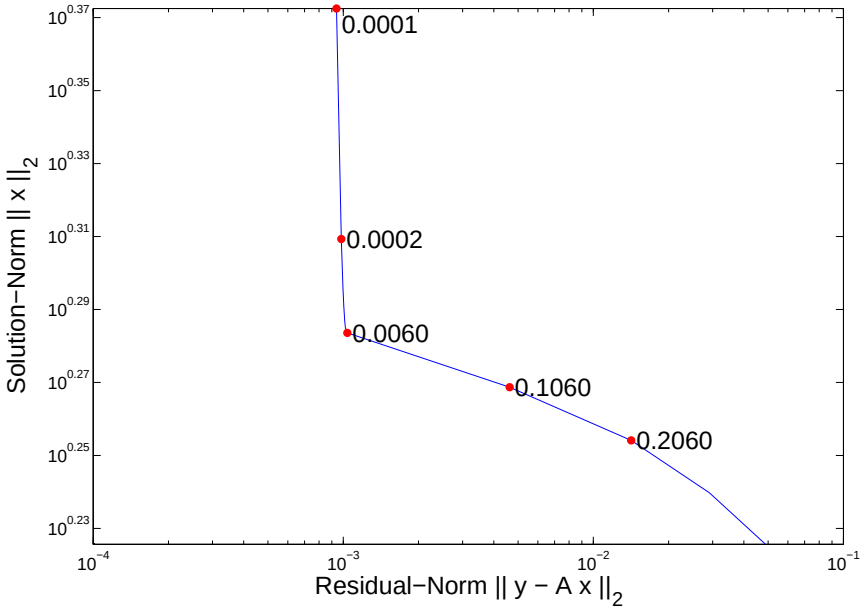

Figure 4.2: *The L-curve for the small example*

Obviously this solution is worthless since it deviates strongly from the exact solution $\bar{\mathbf{x}}^{\mathrm{T}} = (1\ 1)$. The reason is that the design matrix $\mathbf{A}$ in this case has column linearity, which makes itself near rank-deficient, i.e., ill-conditioned. We now apply the L-curve criterion to obtain the Tikhonov-regularized least-squares solution. Normally the set of pre-defined values of regularization parameter is selected according to the size of the values in the normal equations matrix $\mathbf{N}$. Here, we choose 65 values ranging from 0.0001 to 0.5 as regularization parameters for this small example. Figure 4.2 displays the L-curve and from this graph we can find the optimal regularization parameter $\lambda_{\mathrm{opt}} = 0.006$ at the "corner" and compute the

corresponding solution:

$$\hat{\mathbf{x}}_{0.006} = \begin{pmatrix} 1.18 \\ 0.73 \end{pmatrix}$$

We can see that this solution is fairly close to the desired exact solution $\bar{\mathbf{x}}^{\mathrm{T}} = (1\ 1)$.

Chapter 5

Simulation Studies

In order to evaluate the performance of the proposed methodologies, we conducted a series of closed-loop simulation studies. The idea of closed-loop simulation is: we define some point-mass variations in a certain area on the Earth's surface, which generates gravitational deviations at satellite altitude; Then we use these artificially simulated gravitational signals as observations for the observation equations to determinate the point-mass variations in the area. The sequence of this simulation, from point-mass variations to the gravitational signals at space locations and then back to point-mass variations on the Earth's surface, is a closed-loop.

5.1 Area determination

To conduct the closed-loop simulations, firstly we need to define an area on the Earth's surface and a set of point-mass variations in this area. Since our research is based on Greenland, we just choose Greenland as the area on the Earth's surface for our simulation studies. We can select the area with the polygon tool in Google Earth, which is shown in Figure 5.1.

Correspondingly we also need to determine an area at satellite altitude including the space locations of our simulated observations. A point-mass variation on the Earth's surface can theoretically cause gravitational signals at every single point in space. But we don't need too many simulated observations and the signals at the points too far away are too small to be taken into account. Here we can conduct a small experiment to determine the delineation of the area for the simulated observations at satellite altitude. We define a point-mass change on the south-east coast of Greenland. The variation of this change is defined as -5 Gt. Then we compute the gravitational deviations caused by this point-mass change at 40962 points at satellite altitude. These points are homogeneously worldwide distributed. Figure 5.2 displays the result of this experiment. The green point is the position of the point-mass variation on the Earth's surface. The blue points are the positions of calculated gravitational signals at satellite altitude (500 km). From Figure 5.2 we can find that when the distance between the projection on the Earth's surface of the point at satellite altitude and the terrestrial mass point is more than a certain value, the gravitational signals become relatively small. With the help of the distance measurement tool in Google Earth, we can figure out that this distance is around 300 km.

Figure 5.1: *The chosen area over Greenland (Google, 2017)*

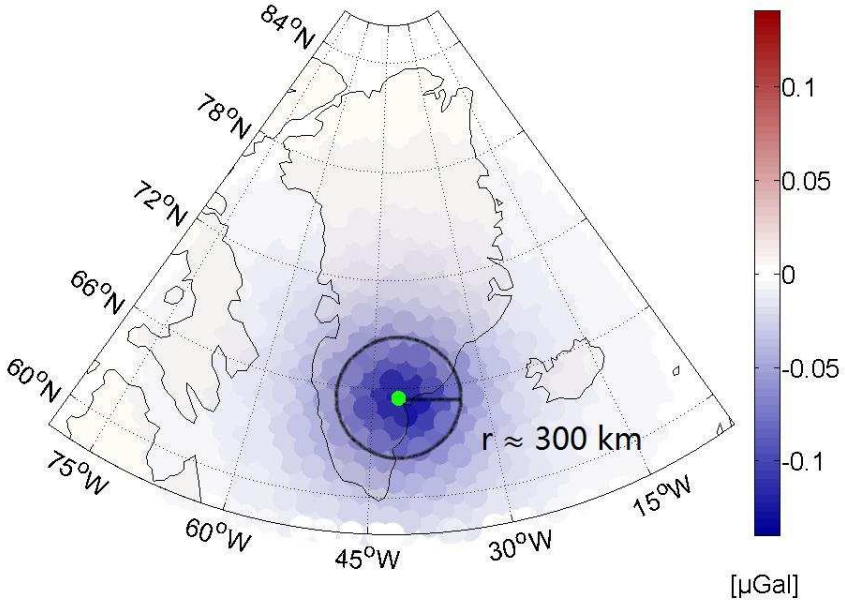

Figure 5.2: *The gravitational deviations at satellite altitude (500 km) caused by one point-mass variation (dm=-5 Gt)*

According to this small experiment, we can determine an area for the simulated observations at satellite altitude, whose projection on the Earth's surface is similar with the Greenland area but only around 300 km extended. With the polygon tool in Google Earth we can select this desired area, which is shown in Figure 5.3.

Figure 5.3: *The projection on the Earth's surface of the chosen area for simulated observations at satellite altitude (Google, 2017)*

5.2 Determination of the distribution density for terrestrial mass points and space locations

After determining the area on the Earth's surface and the area for space locations at satellite altitude, we need to respectively define a set of points in both areas as terrestrial locations of unknowns and space locations of observations. For this purpose, I apply a MATLAB function with 8 polygon files, which are kindly provided by my supervisor Matthias Roth. The 8 polygon files model the Earth's surface using homogeneous points at 8 different levels of resolution. The amount of the points at one level is four times more than that at last level. For example, the level 6 polygon file models the Earth's surface with 10242 homogeneous points and the level 7 with 40962 homogeneous points. When we focus on a certain area on the Earth's surface, we can apply the MATLAB function to pick the desired points in this area from all the

homogeneous modelling points at the defined level. The area can be selected in Google Earth like Figure 5.1 and 5.3 and used as input for the function. So combining the function and the polygon files, we can generate homogeneous points with spherical polar coordinates (λ, ϕ) in a certain area at 8 different levels of distribution density. The higher level we use, the more points we generate in a certain area. Figure 5.4 demonstrates the generation result of level 5-8 in the same area shown in Figure 5.1. Since the resolution of level 1-5 is not enough for our studies and level 8 is too high costing too much calculation time, we apply level 6 and level 7 for our following studies.

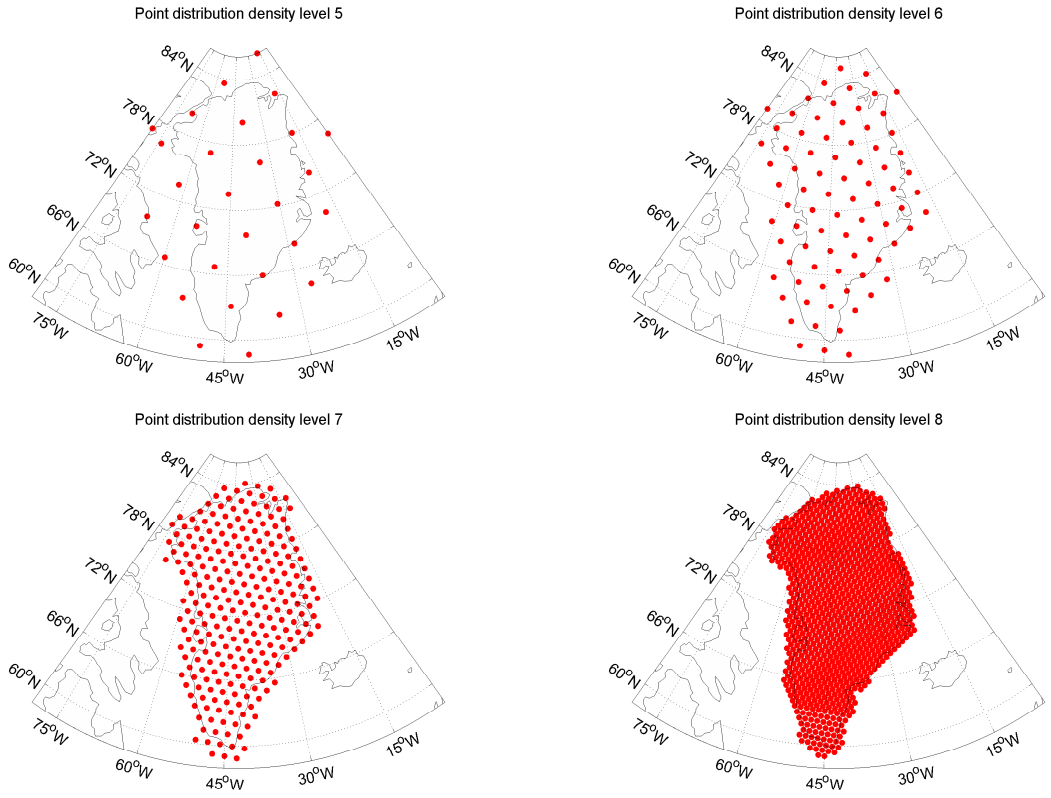

Figure 5.4: *level 5-8 of point distribution density*

5.3 Noise-free simulation

After choosing the areas and the levels of distribution density for mass points and space locations at satellite altitude, we can start to perform our simulation studies. In this section we conduct two noise-free simulations and the difference is the distribution density of mass points on the Earth's surface. The first one is performed with the distribution density level 6 for the terrestrial mass points and the second one with level 7. Considering that the number of observations should be bigger than the number of unknowns, we define that the distribution density for space locations in all the following simulation studies is always level 7. Since the annual ice-mass decline from April 2002 to March 2009 over Greenland is about 299 km^3/year

and the mass loss happened almost on the border of Greenland (Baur, O. and Sneeuw, N., 2011), we define a total mass loss of 300 Gt for our simulations. We randomly distribute the total mass loss at the mass points on the border of Greenland and distribute no mass change at the mass points inside.

5.3.1 Noise-free simulation for low mass point distribution density

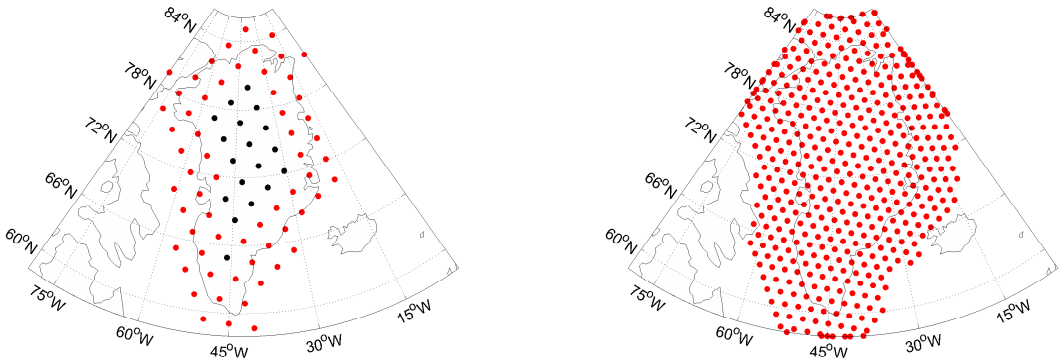

Figure 5.5: *The distribution of the defined mass points over Greenland (80) and the space locations at satellite altitude of simulated observations (464)*

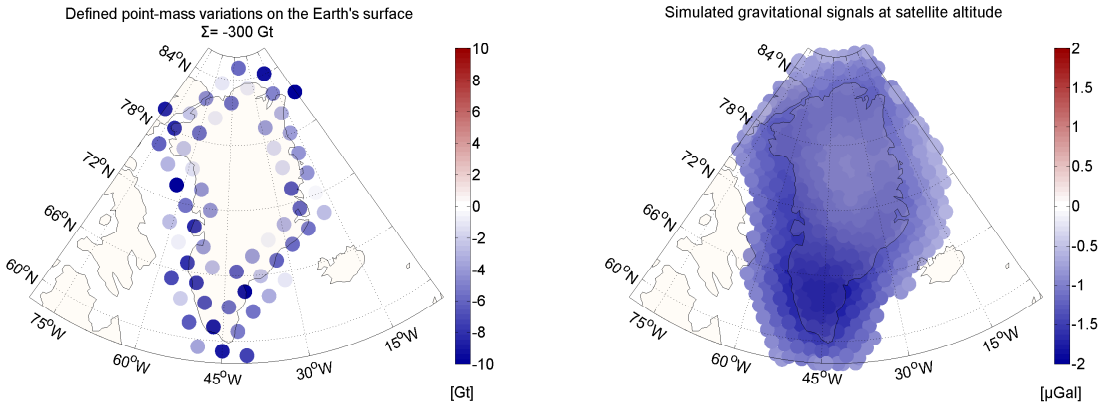

Figure 5.6: *The defined point-mass variations on the Earth's surface (62) and the corresponding gravitational signals at satellite altitude (464)*

Firstly we conduct the noise-free simulation with the distribution density level 6 for the terrestrial mass points. 80 terrestrial mass points are generated over the Greenland area: 62 mass points on the border and 18 mass points inside. Then we define random mass changes at the 62 mass points on the border. The individual magnitudes range from -0.23 Gt to -9.95 Gt. Meanwhile we define no mass change at the 18 mass points inside. The total mass change of these defined 80 mass points is -300 Gt. The left panel of Figure 5.5 displays the distribution of these defined mass points over Greenland. The red points represent the 62 mass points with mass change and the black points represent the 18 mass points without mass change. Correspondingly applying the distribution density level 7 we generate 464 space locations at satellite

altitude in the chosen area shown in Figure 5.3 for the simulated observations. The right panel of Figure 5.5 displays the distribution of these space locations. According to Equation (3.4), we can compute the simulated gravitational signals from the 62 defined point-mass variations. Figure 5.6 illustrates the defined point-mass variations on the Earth's surface and the corresponding gravitational signals at satellite altitude.

Then we use these 464 simulated gravitational signals as the observations for the inversion and the unknowns are the mass variations of the 80 mass points on the Earth's surface. Since there is no noise added to the simulated observations, we can take the weight matrix $\mathbf{P}$ as an identity matrix $\mathbf{I}$. Firstly we apply Gauss-Markov model to obtain the ordinary least-squares solution, which is displayed in Figure 5.7. From Figure 5.7 we can see that the ordinary least-squares solution is relatively good compared with the defined point-mass variations shown in the left panel of Figure 5.6. The numerical result also indicates that the ordinary least-squares solution is pretty good since the sum of the solution is -300.00 Gt and the error is only around 1.49×10^{-5} Gt.

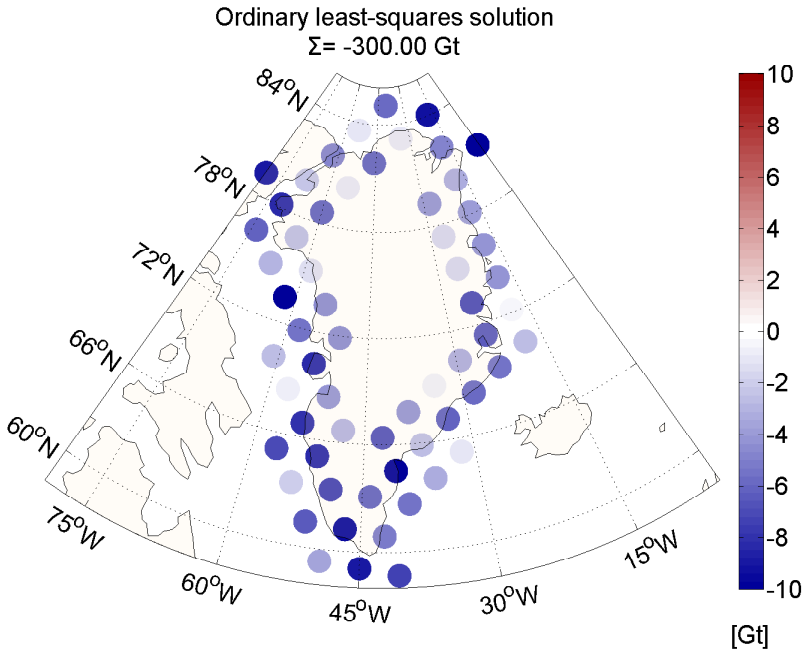

Figure 5.7: *The ordinary least-squares solution of the noise-free simulation for low mass point distribution density*

However, we still apply Tikhonov regularization for the inversion in this simulation to see the result. According to the size of the values in normal matrix $\mathbf{N}$, here we define 300 discrete regularization parameters, ranging from 1.0×10^{-28} to 1.0×10^{-20} for this adjustment and also for all the other following adjustments in this thesis. Figure 5.8 is the graph plotting the solution norm against residual norm for the noise-free simulation for low mass point distribution density, which is not a typically L-shaped graph. Then we select 4 regularization parameters along this graph ($\lambda_1 = 1.00 \times 10^{-28}, \lambda_2 = 4.03 \times 10^{-27}, \lambda_3 = 1.91 \times 10^{-24}, \lambda_4 = 9.05 \times 10^{-22}$) and calculate the corresponding Tikhonov-regularized least-squares solutions and also the errors compared with defined values. The result is illustrated in Figure 5.9. The first panel of each row is the position on the curve and the value of the regularization parameter; the second

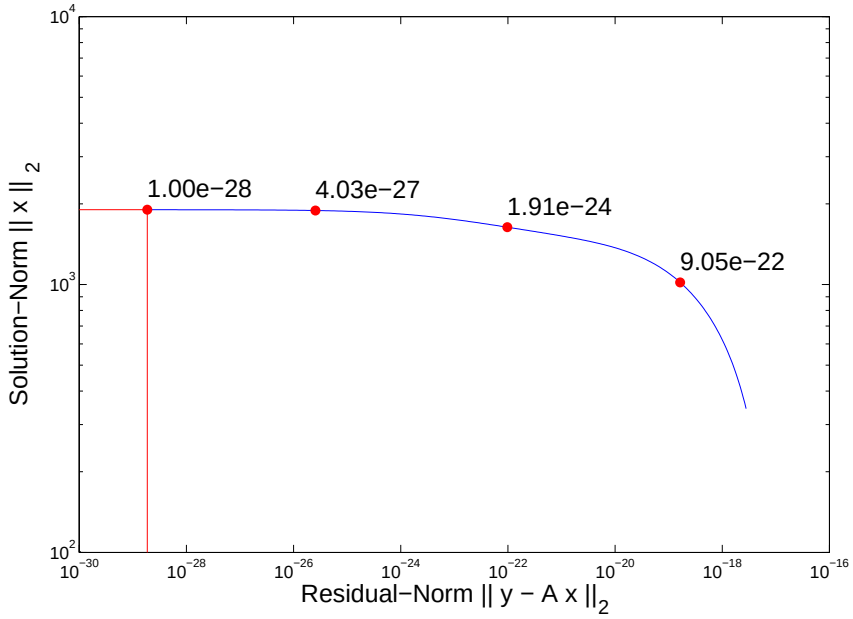

Figure 5.8: *The graph plotting the solution norm against residual norm of the noise-free simulation for low mass point distribution density*

panel is the corresponding Tikhonov-regularized solution; the third panel is the distribution of the errors for individual mass variations compared with the defined values. Table 5.1 is the summary of the result. From the result of the simulation, we can find that the solution becomes better when the regularization parameter is smaller. The theoretical smallest regularization parameter is 0, so the optimal solution is just the ordinary least-squares solution obtained with Gauss-Markov model, which can also be verified by the result of our previous experiment using Gauss-Markov model.

Test	λ	$\sum$ dm	Error	Error in percent
1	1.00×10^{-28}	-300.00 Gt	< 0.0001 Gt	< 0.01%
2	4.03×10^{-27}	-300.00 Gt	0.0017 Gt	< 0.01%
3	1.91×10^{-24}	-299.99 Gt	0.0147 Gt	< 0.01%
4	9.05×10^{-22}	-269.75 Gt	30.2456 Gt	10.08%

Table 5.1: *The summary of the noise-free simulation for low mass point distribution density*

Finally we can draw a conclusion for the first simulation: when the density of the mass point distribution is low and the observations are noise-free, the ordinary least-squares solution is stable and optimal. In this case the Tikhonov regularization is not necessary for the adjustment.

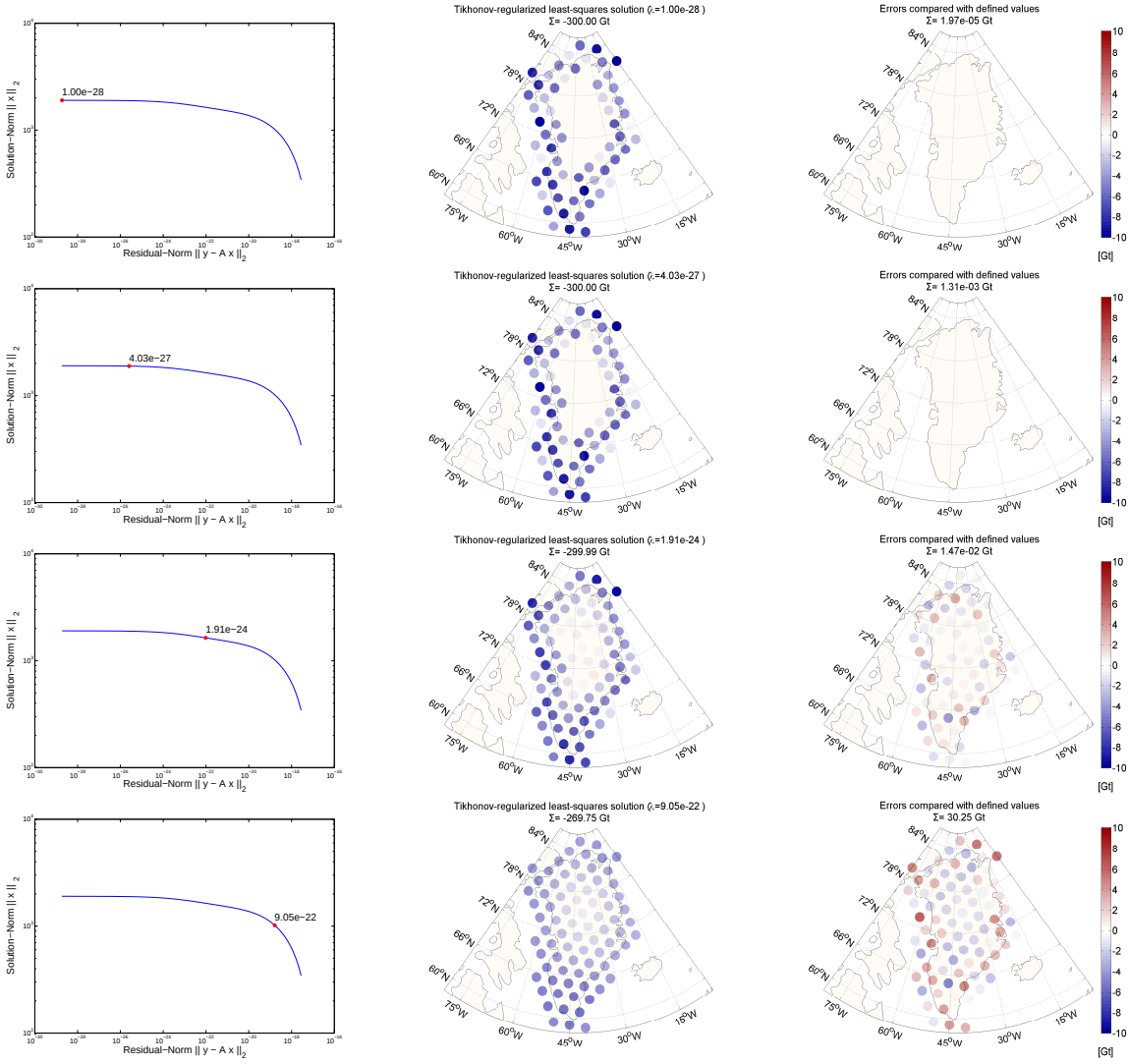

Figure 5.9: *The Tikhonov-regularized least-squares solutions of the noise-free simulation for low mass point distribution density*

5.3.2 Noise-free simulation for high mass point distribution density

Then we conduct the same noise-free simulation as section 5.2.1 but with level 7 distribution density for the terrestrial mass points. This time 256 mass points are generated over the Greenland area: 128 mass points on the border and 128 mass points inside. We also define random mass changes at the 128 mass points on the border and no mass change at the other interior mass points. The individual magnitudes of the mass changes range from -0.09 Gt to -4.59 Gt. The total mass change of these 128 mass points is still 300 Gt. The left panel of Figure 5.10 displays the distribution of these defined mass points over Greenland. The red points represent the 128 mass points with mass change and the black points represent the other 128 mass points without mass change. Correspondingly we also distribute 464 space locations at satellite altitude for the simulated observations, which is displayed in the right panel of Figure 5.10. According to Equation (3.4), we compute the simulated gravitational signals generated from the 128 defined point-mass variations. Figure 5.11 illustrates the defined point-mass variations on the Earth's surface and the corresponding gravitational signals at satellite altitude.

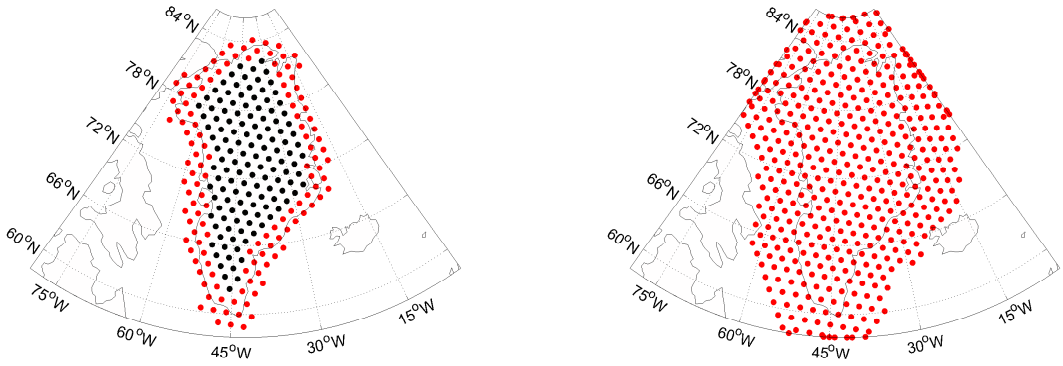

Figure 5.10: *The distribution of the defined mass points over Greenland (256) and the space locations at satellite altitude of simulated observations (464)*

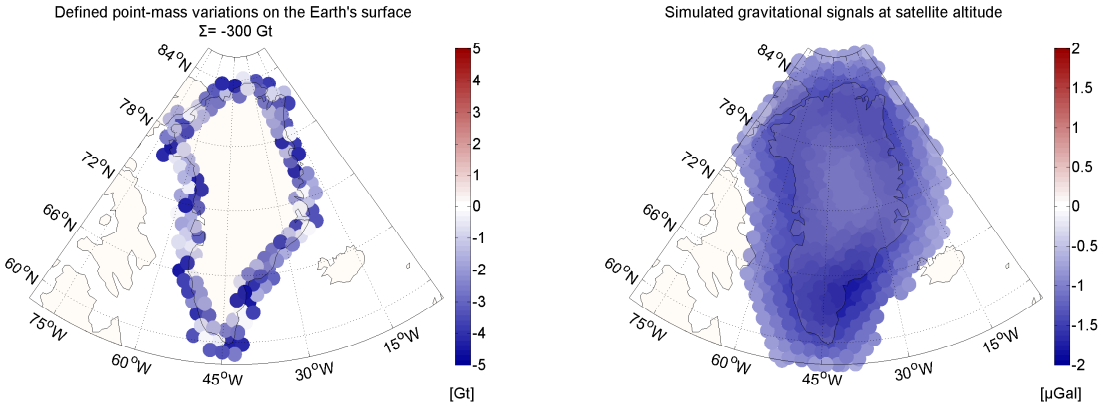

Figure 5.11: *The defined point-mass variations on the Earth's surface (128) and the corresponding gravitational signals at satellite altitude (464)*

Then we use the 464 simulated gravitational signals as the observations for the inversion and the unknowns are the mass variations of the 256 mass points on the Earth's surface. We still apply Gauss-Markov to obtain the ordinary least-squares solution first and Figure 5.12 indicates the result. Obviously this solution is worthless because in this simulation the density of the mass point distribution is much higher, in other words the mass points are very close to each other, which makes the design matrix $\mathbf{A}$ rank-deficient, i.e., ill-conditioned. So in this case the Tikhonov regularization is necessary for the adjustment.

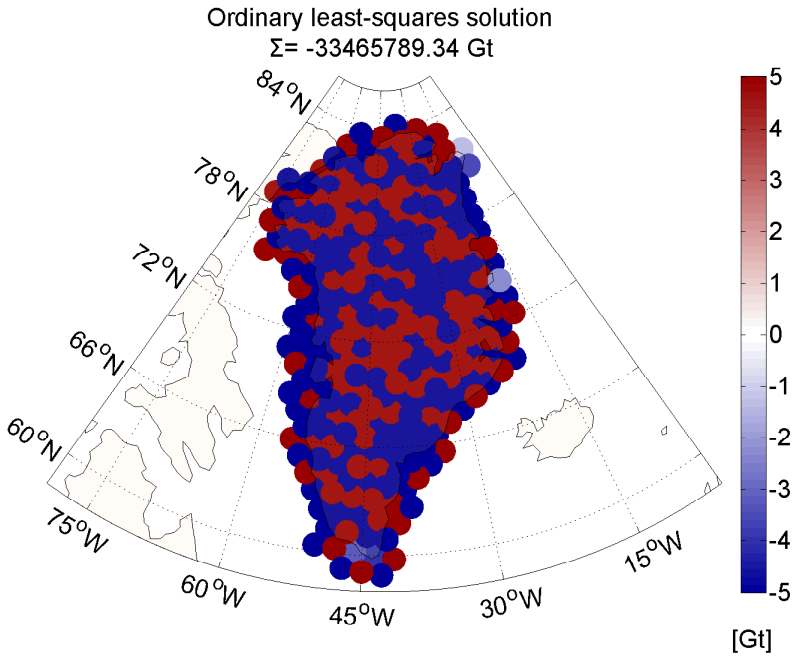

Figure 5.12: *The ordinary least-squares solution of the noise-free simulation for high mass point distribution density*

Figure 5.13 is the graph plotting the solution norm against residual norm, which is not a typically L-shaped graph. However, there is also a "corner" separating the two parts in this graph and the difference from the typical L-curve is the direction of the upper part. In a typical L-curve, the upper part is more or less vertical and the direction is pointing up, which means the sharp increase of the solution norm and the slow increase of the residual norm. While in this graph, although the upper part is not smooth, it is more or less horizontal and the direction is pointing right, which means the sharp increase of the residual norm and slow increase of solution norm. Since the idea of the L-curve criterion is finding the compromise between minimization of the solution norm and the residual norm, we guess that this "corner" can still provide the optimal regularization parameter for the adjustment. Then we select 5 regularization parameters, two along each part of the curve and one at the "corner" and compute the respective solutions to prove our guess. The 5 selected regularization parameters are: $\lambda_1 = 3.88 \times 10^{-28}, \lambda_2 = 1.50 \times 10^{-27}, \lambda_3 = 9.55 \times 10^{-27}, \lambda_4 = 4.52 \times 10^{-24}, \lambda_5 = 3.38 \times 10^{-22}$. Their positions in the graph are also displayed in Figure 5.13.

The result is illustrated in Figure 5.14. The first panel of each row is the position on the curve and the value of the regularization parameter; the second panel is the corresponding Tikhonov-regularized solution; the third panel is the distribution of the errors for individual mass varia-

tions compared with the defined values. Table 5.2 is the summary of the result.

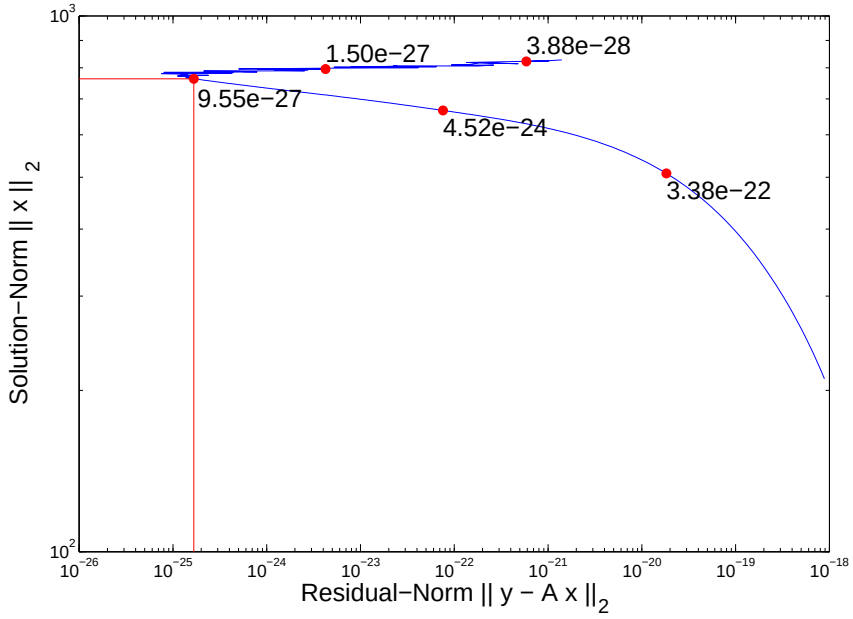

Figure 5.13: *The graph plotting the solution norm against residual norm of the noise-free simulation for high mass point distribution density*

Test	λ	$\sum$ dm	Error	Error in percent
1	3.88×10^{-28}	-300.63 Gt	(-)0.6328 Gt	0.21%
2	1.50×10^{-27}	-299.93 Gt	0.0712 Gt	0.02%
3	9.55×10^{-27}	-299.99 Gt	0.0063 Gt	< 0.01%
4	4.52×10^{-24}	-299.93 Gt	0.0658 Gt	0.02%
5	3.38×10^{-22}	-291.93 Gt	8.0670 Gt	2.69%

Table 5.2: *The summary of the noise-free simulation for high mass point distribution density*

From the result we can verify our guess and draw a conclusion: the optimal regularization parameter for this simulation is at the "corner" of the graph even though it is not a typical L-shaped curve. When we apply a smaller regularization parameter, the total mass change is close to the defined value -300 Gt but the individual errors increase specially at those interior mass points; when we apply a bigger regularization parameter, the solution appears over-smooth and the sum of errors also increase.

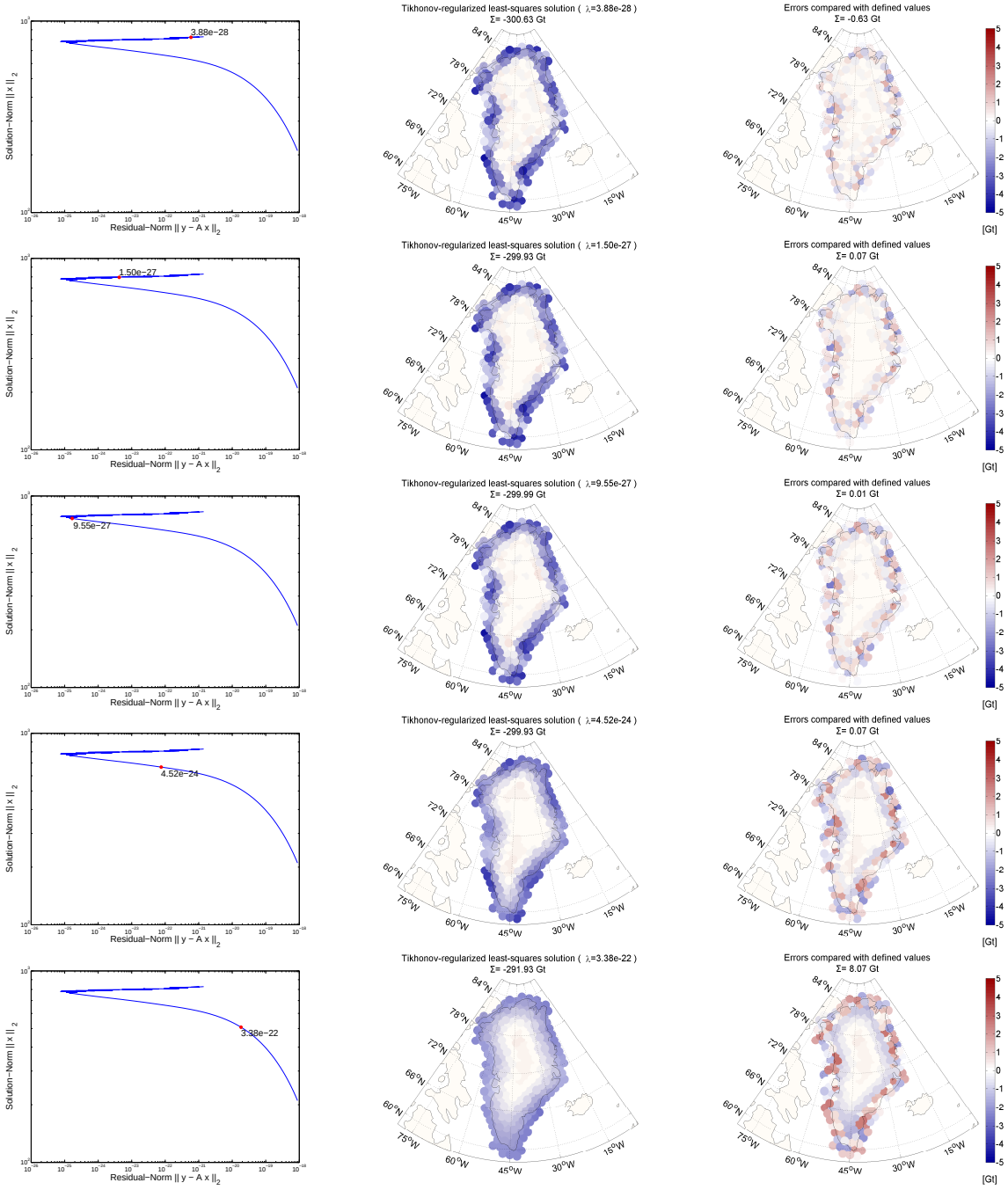

Figure 5.14: *The Tikhonov-regularized least-squares solutions of the noise-free simulation for high mass point distribution density*

5.4 Simulation with noise

In this section, we conduct the closed-loop simulations again as in section 5.2, but the difference is that noise is considered and added to the generated gravitational signals and together form the simulated observations for the inversion. The estimation of the noise is based on GRACE data. According to Equation (2.3) and the law of error propagation, we can calculate the variance of dg ($\hat{\sigma}_{dg}$) using the variances of spherical harmonic coefficients ($\sigma_{\bar{c}_{lm}}$, $\sigma_{\bar{s}_{lm}}$) provided by the GRACE data. Then we define $\hat{\sigma}_{dg}$ as the variances for the generated gravitational signals and multiply them with normally distributed random numbers ($\mu = 0$, $\sigma = 0.5$) to generate the noise for the simulated observations, which makes the random noises also normally distributed ($\mu = 0$, $\sigma \approx 0.04$ μGal). The individual magnitudes of the generated noise range from -0.136 μGal to 0.141 μ Gal.

5.4.1 Simulation with noise for low mass point distribution density

Here, we use the same mass point distribution and defined point-mass variations as in section 5.2.1, which are already displayed in Figure 5.5 and 5.6. The only difference is that we add the generated noise to the gravitational signals to form the observations with noise for the inversion. The left panel of Figure 5.15 shows the defined point-mass variations (same as the left panel of Figure 6.6); the right panel indicates the simulated observations including noise.

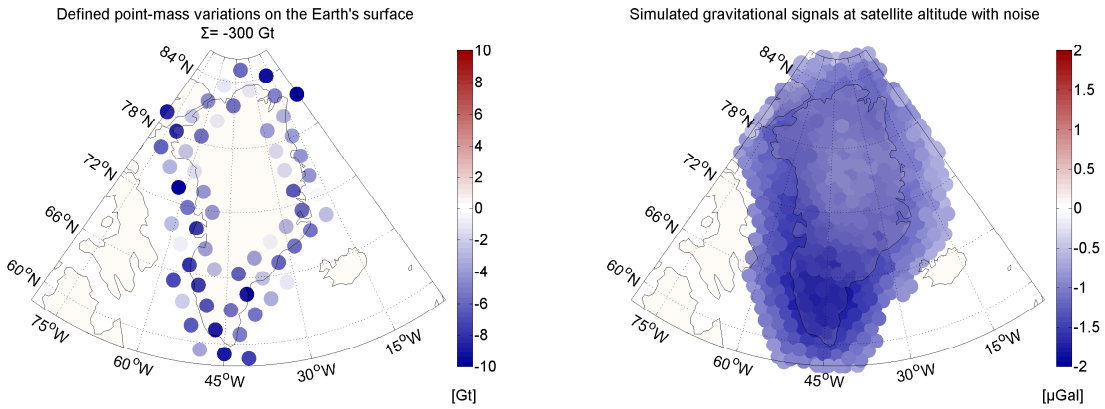

Figure 5.15: *The defined point-mass variations on the Earth's surface (62) and the corresponding gravitational signals including noise at satellite altitude (464)*

Same as section 5.2.1, we apply Gauss-Morkov model first to obtain the ordinary least-squares solution. The result is displayed in Figure 5.16, which is obviously worthless even though the numerical result of total mass change (-298.83 Gt) is close to the true value (-300 Gt). The error of the individual point-mass variations is fairly big compared with the defined values shown in the left panel of Figure 5.15. The result of applying Gauss-Morkov model indicates that the ordinary least-squares solution becomes relatively unstable when there are noises included in the observations, even if the distribution density of the mass points is low.

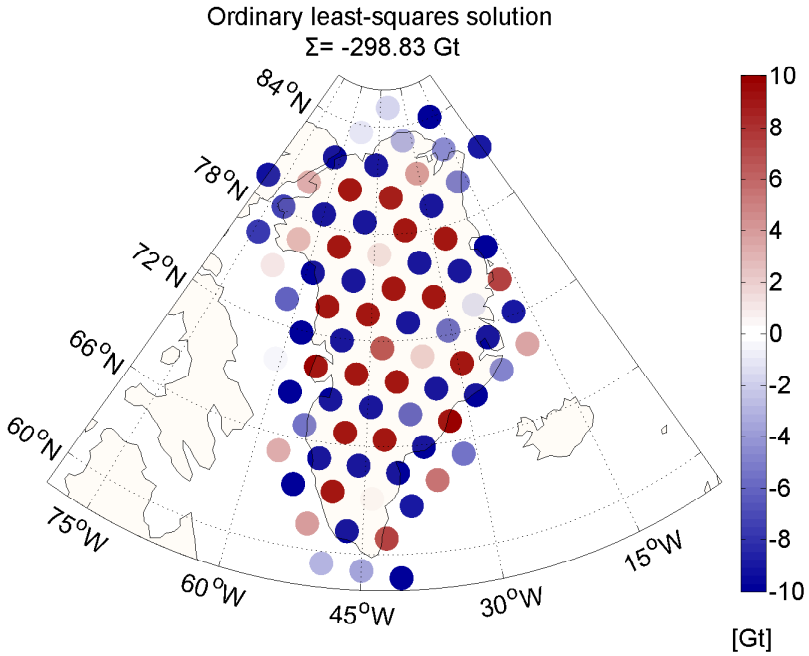

Figure 5.16: *The ordinary least-squares solution of the simulation with noise for low mass point distribution density*

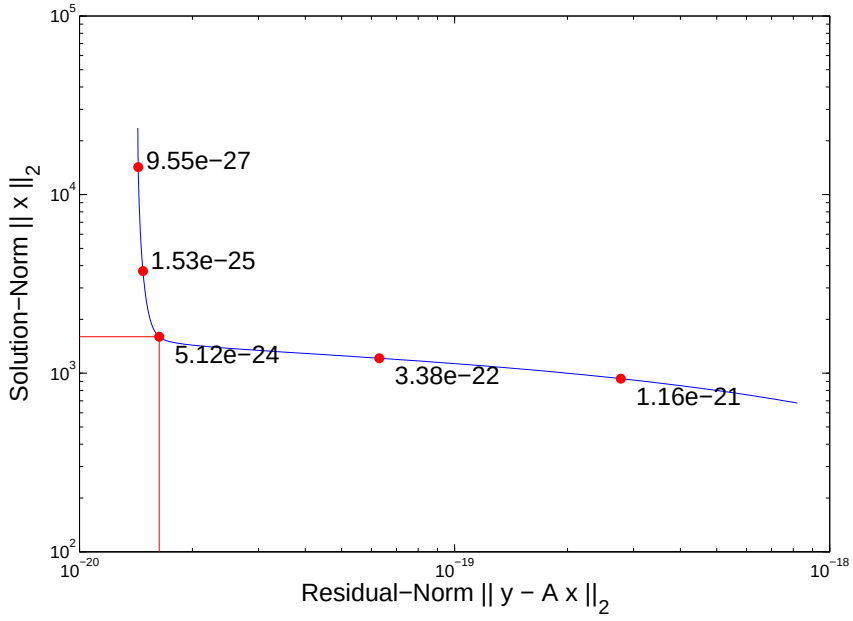

Figure 5.17: *The graph plotting the solution norm against residual norm of the simulation with noise for low mass point distribution density*

Then we apply Tikhonov regularization for the adjustment. Figure 5.17 represents the graph plotting the solution norm against residual norm for this adjustment, which is a typically L-shaped curve. Then we select 5 regularization parameters and calculate the corresponding Tikhonov-regularized least-squares solutions and the errors compared with defined values. The 5 parameters are: $\lambda_1 = 9.55 \times 10^{-27}, \lambda_2 = 1.53 \times 10^{-25}, \lambda_3 = 5.12 \times 10^{-24}, \lambda_4 = 3.38 \times 10^{-22}, \lambda_5 = 1.16 \times 10^{-21}$. λ_3 is the parameter at the "corner" of the L-curve, which is considered as the optimal regularization parameter. The positions of these 5 selected regularization parameters in the graph are also displayed in Figure 5.17.

The inversion result is illustrated in Figure 5.18. The first panel of each row is the position on the curve and the value of the regularization parameter; the second panel is the corresponding Tikhonov-regularized solution; the third panel is the distribution of the errors for individual mass variations compared with the defined values. Table 5.3 is the summary the result.

Test	λ	$\sum$ dm	Error	Error in percent
1	9.55×10^{-27}	-298.91 Gt	1.0946 Gt	0.36%
2	1.53×10^{-25}	-299.34 Gt	0.6607 Gt	0.22%
3	5.12×10^{-24}	-299.82 Gt	0.1821 Gt	0.06%
4	3.38×10^{-22}	-285.59 Gt	14.4082 Gt	4.80%
5	1.16×10^{-21}	-261.90 Gt	38.0893 Gt	12.70%

Table 5.3: *The summary of the simulation with noise for low mass point distribution density*

From the result we can find that the optimal solution is obtained with the optimal regularization parameter at the "corner" of the L-curve. When smaller regularization parameters are applied for the adjustment, the numerical total change of point-mass variations is relatively good, but the error of individual point-mass variations is fairly big, which leads to a completely different distribution of point-mass variations over the whole area. The first and second rows of Figure 5.18 are the example illustration for this fact. When bigger regularization parameters are applied for the adjustment, the numerical result of total mass change becomes worse and the differences between the point-mass variations become smaller, which leads to over-smooth solutions. The fourth and fifth rows of Figure 5.18 are the examples that demonstrate this fact.

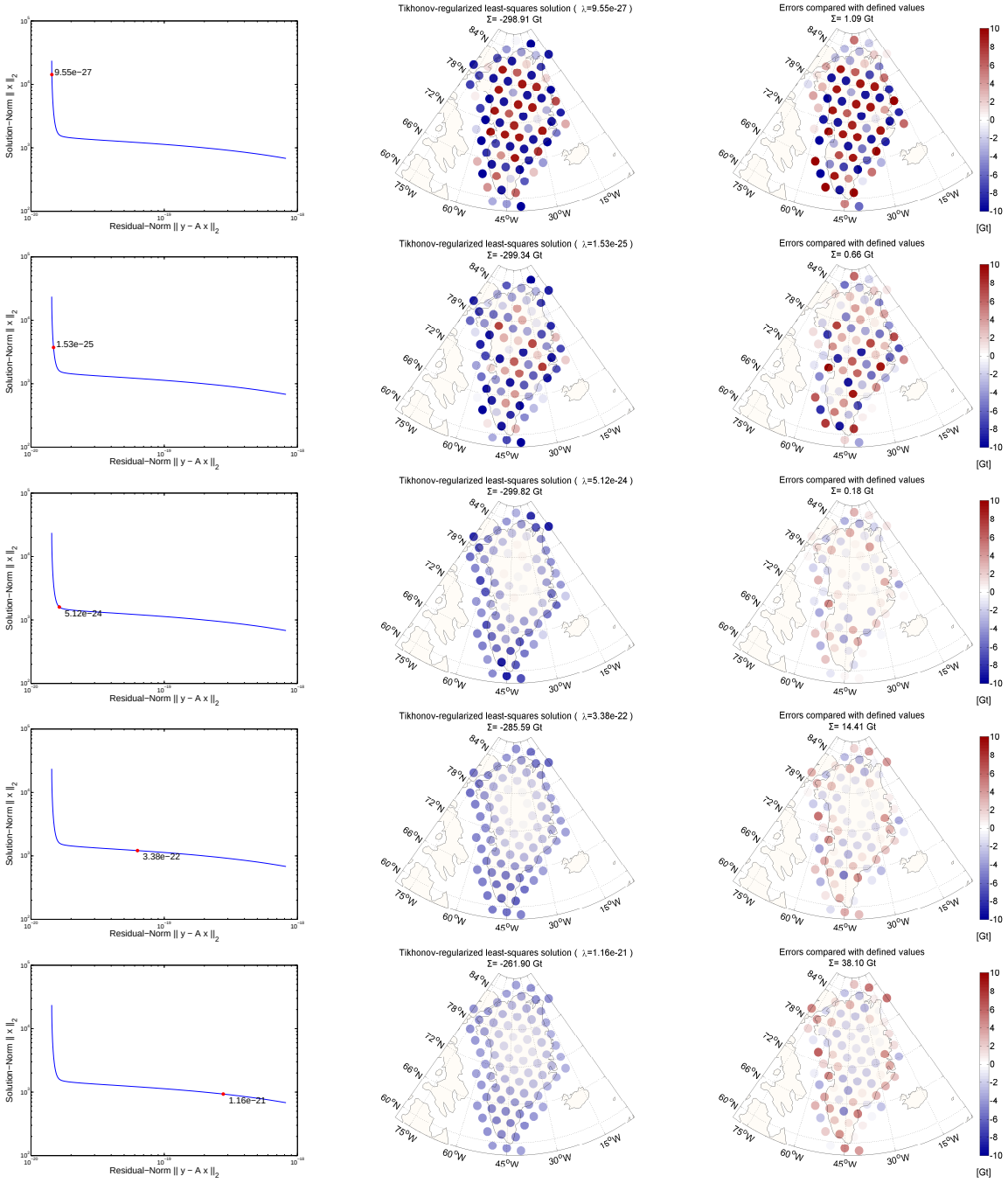

Figure 5.18: *The Tikhonov-regularized least-squares solutions of the simulation with noise for low mass point distribution density*

5.4.2 Simulation with noise for high mass point distribution density

Then we perform the same simulation as in section 5.3.1 but for high mass point distribution density. The mass point distribution and defined point-mass variations are same as those in section 5.2.2. The left panel of Figure 5.19 shows the defined point-mass variations (same as the left panel of Figure 5.11); the right panel indicates the simulated observations including noise.

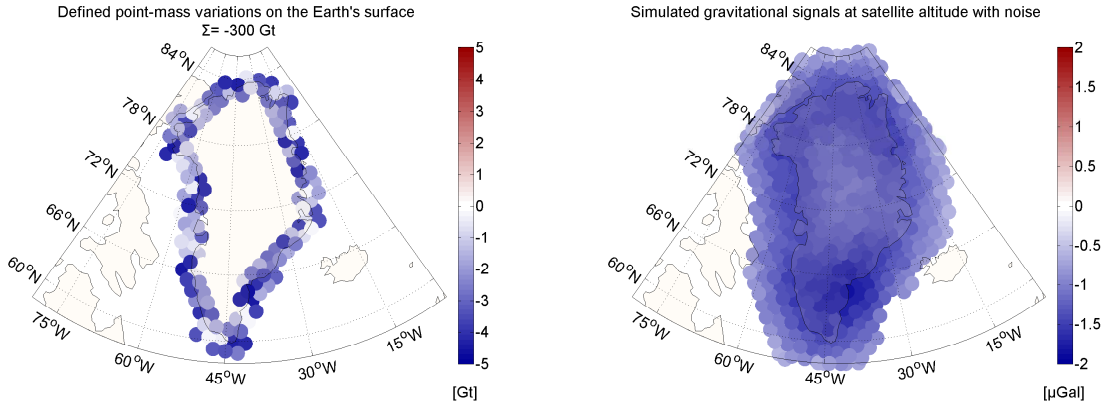

Figure 5.19: *The defined point-mass variations on the Earth's surface (128) and the corresponding gravitational signals including noise at satellite altitude (464)*

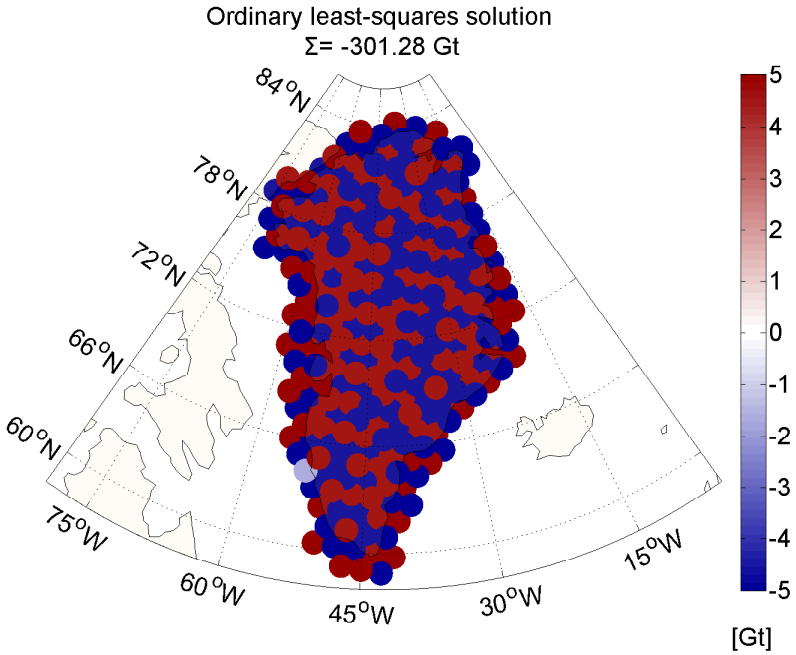

Figure 5.20: *The ordinary least-squares solution of the simulation with noise for high mass point distribution density*

Here we still apply Gauss-Morkov model first to get the ordinary least-squares solution, which is displayed in Figure 5.20. Obviously this solution is completely different from the defined mass-point variations. The solution obtained with Gauss-Morkov model is unstable when the high distribution density of mass points makes the design matrix **A** ill-conditioned, which is already explained in section 5.2.2.

Then we apply Tikhonov regularization for the adjustment. Figure 5.21 represents the graph plotting the solution norm against residual norm for this adjustment, which is a typically L-shaped curve. Then we select 5 regularization parameters and compute the corresponding Tikhonov-regularized least-squares solutions and also the errors compared with defined values. The 5 parameters are: $\lambda_1 = 9.55 \times 10^{-27}, \lambda_2 = 1.53 \times 10^{-25}, \lambda_3 = 6.16 \times 10^{-24}, \lambda_4 = 3.38 \times 10^{-22}, \lambda_5 = 1.16 \times 10^{-21}$. λ_3 is the parameter at the "corner" of the L-curve, which is considered to be the optimal regularization parameter. The positions of these 5 selected regularization parameters are displayed in Figure 5.21.

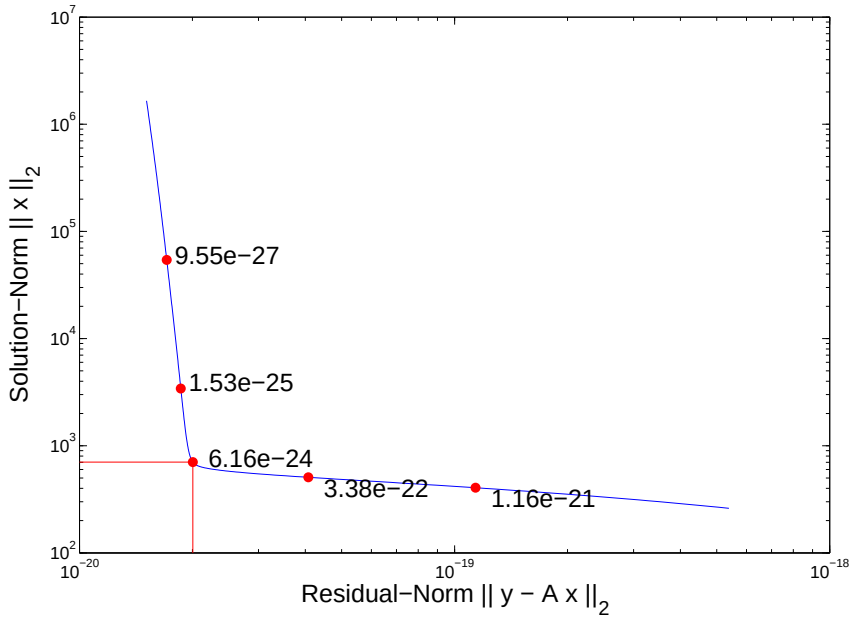

Figure 5.21: *The graph plotting the solution norm against residual norm of the simulation with noise for high mass point distribution density*

Test	λ	$\sum$ dm	Error	Error in percent
1	9.55×10^{-27}	-299.32 Gt	0.6784 Gt	0.23%
2	1.53×10^{-25}	-299.59 Gt	0.4132 Gt	0.14%
3	6.16×10^{-24}	-299.87 Gt	0.1329 Gt	0.04%
4	3.38×10^{-22}	-291.93 Gt	8.0711 Gt	2.69%
5	1.16×10^{-21}	-280.15 Gt	19.8466 Gt	6.62%

Table 5.4: *The summary of the simulation with noise for high mass point distribution density*

The inversion result is illustrated in Figure 5.22. The first panel of each row is the position on the curve and the value of the regularization parameter; the second panel is the corresponding

Tikhonov-regularized solution; the third panel is the distribution of the errors for individual mass variations compared with the defined values. Table 5.4 is the summary the result.

From the result we can find that the optimal solution is obtained with the optimal regularization parameter at the "corner" of the L-curve. When smaller regularization parameters are applied for the adjustment, the numerical result of total mass change is relatively good, but the errors for single point-mass variations is fairly big, which leads to a completely different distribution of point-mass variations over the whole area. The first and second rows of Figure 5.22 are the example illustration for this fact. When bigger regularization parameters are applied for the adjustment, the numerical result of total mass change becomes worse and the differences between the point-mass variations become smaller, which leads to over-smooth solutions. The fourth and fifth rows of Figure 5.22 are the examples that demonstrate this fact.

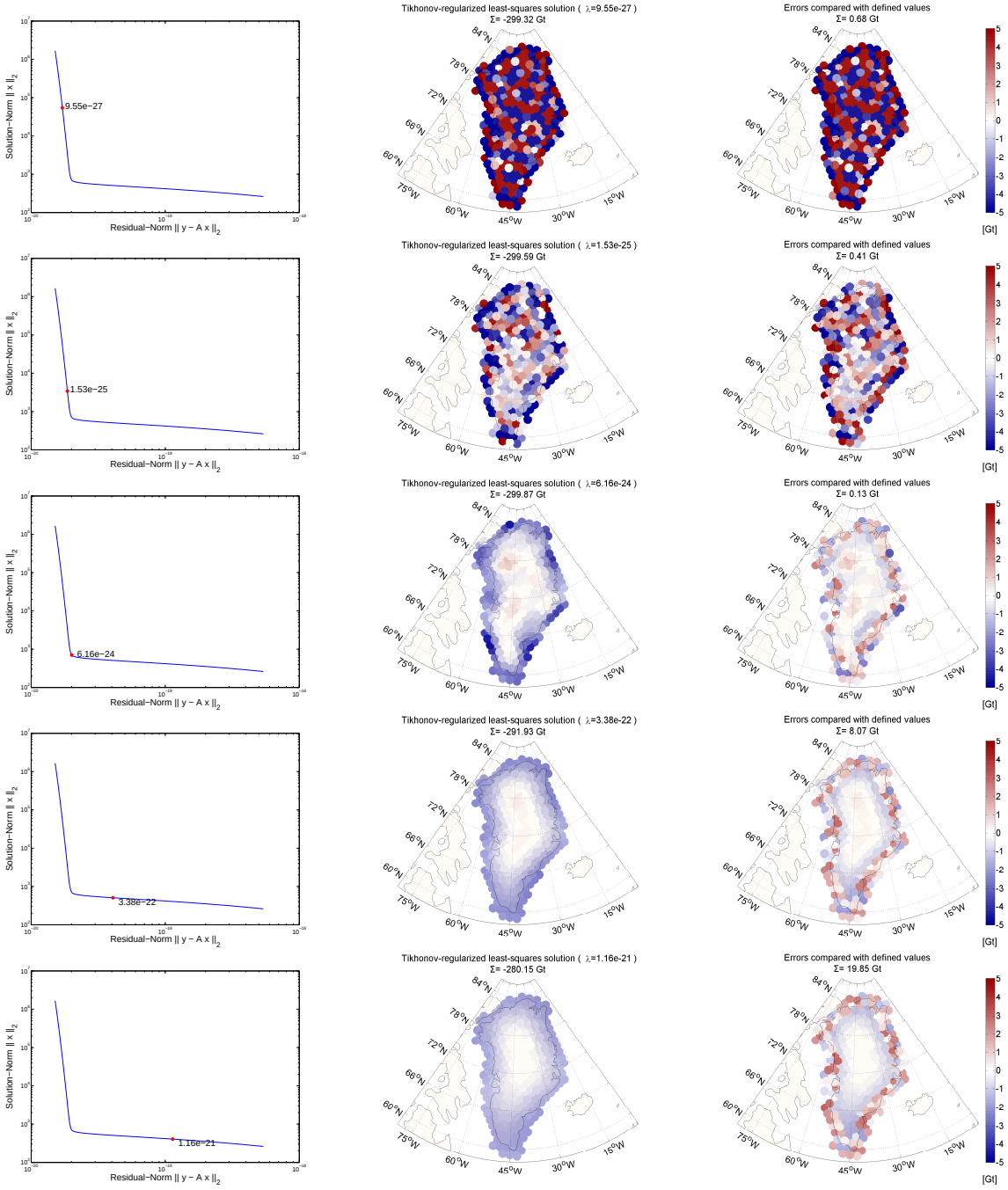

Figure 5.22: *The Tikhonov-regularized least-squares solutions of the simulation with noise for high mass point distribution density*

5.5 The conclusion of the simulation studies

From all these 4 simulation studies we can draw a conclusion for the Gravity inversion on the Greenland area: if the observations are noise-free, Tikhonov regularization is necessary for the least-squares adjustment only when the mass point distribution density is high; if the observations are not noise-free, the ordinary least-squares solution is unstable whether the mass point distribution density is low or high. So Tikhonov regularization is always necessary for stabilizing the least-squares solution when the observations are not noise-free and L-curve criterion is an efficient method to find the proper regularization parameter. This conclusion, drawn from the simulation studies, helps us perform the right steps to conduct the gravity inversion with GRACE-derived observations in the next chapter.

Chapter 6

Experiment using real GRACE data

In chapter 5 we perform the gravity inversion with simulated observations and evaluate the L-curve criterion for Tikhonov regularization. In this chapter we conduct the gravity inversion with the observations derived from real GRACE data to obtain the information of Greenland ice mass loss. From the conclusion drawn in chapter 5, we know that when the observations for the gravity inversion in Greenland are not noise-free, the Tikhonov regularization is always necessary for stabilizing the least-squares solution whether the density of mass point distribution is low or high. Since it is so, we conduct the gravity inversion with high mass point distribution density, i.e., distribution density level 7, which is introduced in section 5.2, to obtain a high resolution spatial mass variation pattern over the Greenland area. Besides, the distribution density of space locations at satellite altitude is still level 7 as in chapter 5.

6.1 Determination of terrestrial mass points and space locations

Since the distribution densities are decided and the research area is the same as the simulation studies in Chapter 5, we can know that the distributions of terrestrial mass points and space locations at satellite altitude for the gravity inversion in this chapter are just those used in section 5.3.2, which are already displayed in Figure 5.10. However, from the left panel of Figure 5.10 we can see that some terrestrial mass points are located offshore, which is not a problem for simulation studies since all the mass variations are defined by ourselves. But in real world these offshore mass points also have mass variations even if they are relatively very small (Baur, O. and Sneeuw, N., 2011). And these variations can become a small influence factor to the total mass change of Greenland. So here in chapter for the gravity inversion using real GRACE data we omit the mass points located offshore. Meanwhile from the right panel of Figure 5.10 we can find that some space locations are very close to Canada and Iceland, and some are even already over the north-east coast of Canada. As a matter of fact, gravitational-change signals are not exclusively concentrated over the area of interest, but also leak to the surrounding regions, strictly speaking over the whole globe. Consequently, signals originating from disturbing sources located outside the recovery area, such as Canada and Iceland, leak into the region of interest and the point-mass modelling approach misleadingly attributes these disturbing signals to be caused by the mass changes inside the recovery area, i.e., Greenland (Baur, O. and Sneeuw, N., 2011). In other words, the gravitational signals at the space locations shown in the right panel of Figure 5.10, specially those close to or even over Canada and Iceland, are not only corresponding to the mass changes in Greenland, but also to the mass changes in Canada and Iceland. However, all the gravitational signals are considered to be

caused only by the mass changes in Greenland and used for the gravity inversion, which leads to some errors in the inversion result. In order to keep the disturbing effects as low as possible, we omit those space locations from the right panel of Figure 5.10, which are close to or even over Canada and Iceland, since the disturbing effect is relatively bigger at these locations and after omitting them we can still have enough observations for the gravity inversion. The determination of terrestrial mass points and space locations after omitting is displayed in Figure 6.1. The first row is the same as Figure 5.10, which indicates the distributions before omitting. The left panel of second row shows the distribution of the terrestrial mass points after omitting, which are the positions of unknown mass variations for the gravity inversion and the amount is 196; the right panel of second row shows the space locations at satellite altitude after omitting, i.e., the positions of the GRACE-derived observations for the gravity inversion in this chapter and the amount is 353.

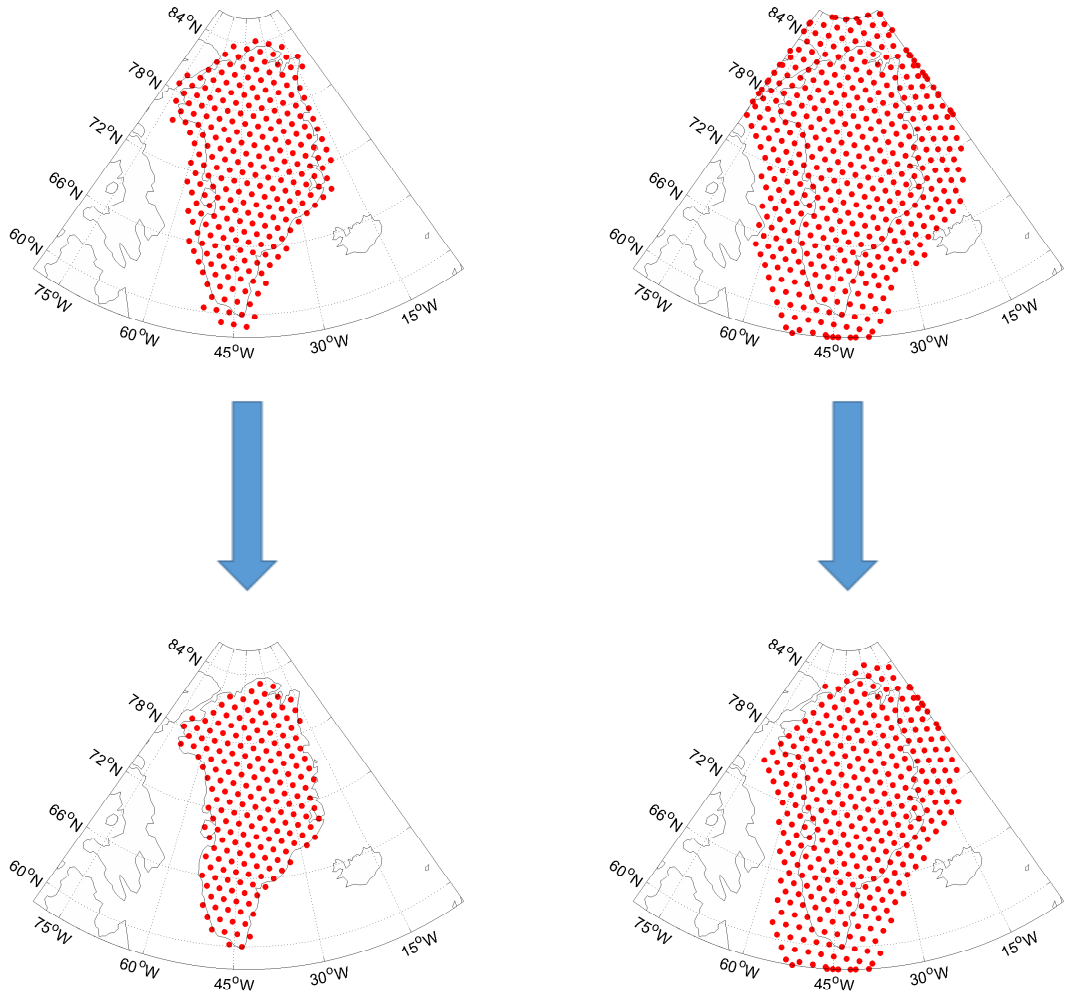

Figure 6.1: *The determination of terrestrial mass points (196) and space locations (353) for the Gravity inversion*

6.2 The gravity inversion process

The determination in the last section offers us the coordinates of both selected terrestrial mass points and space locations at satellite altitude, which enables us to yield the design matrix **A** for the observation equation by means of point-mass modelling. As explained in section 2.2, since we have the coordinates of the selected space locations at satellite altitude and the monthly deviations of spherical harmonic coefficients $d\bar{c}_{lm}$ and $d\bar{s}_{lm}$ derived from GRACE data, according to Equation (2.3) we can compute the monthly gravitational deviations for one space location at satellite altitude. If we perform this calculation for all the 353 selected space locations at satellite altitude shown in the right panel of second row in Figure 6.1, we can obtain a vector with length 353 containing the gravitational deviations of all the space locations at satellite altitude in a specific month, which is just one of the observation vectors for the inversion. In our investigated 14-year sequence from April 2002 to March 2016, there are 155 months with available GRACE data except few months, in which the GRACE data is missing. If we repeat this calculation in every single month, we can obtain 155 observation vectors respectively related to the 155 months in the 14-year sequence, which are displayed in Figure 6.2. $\mathbf{y}_k$ indicates the observation vector of month k. The element $dg_{i,k}$ in the observation vectors indicates the GRACE-derived gravitational deviation at space location i in month k.

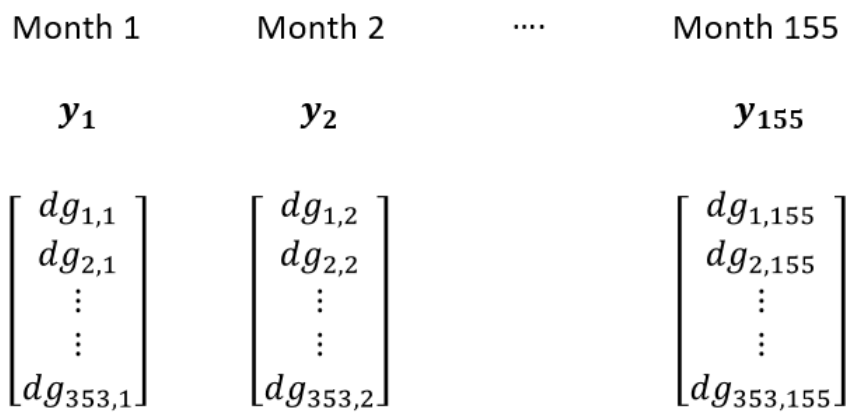

Figure 6.2: *The observation vectors containing GRACE-derived monthly gravitational deviations*

After gaining all the observation vectors we need, we can start to conduct the gravity inversion to obtain the mass deviations by solving the observation equations. Since we have 155 observation vectors, we need to solve 155 corresponding observation equations and obtain 155 unknown vectors. Each of these 155 unknown vectors contains the mass deviations at those 196 selected terrestrial mass points in the corresponding month. This process is demonstrated in Figure 6.3. The solution $\hat{\mathbf{x}}_k$ of each observation equation contains the desired mass deviations at all the 196 selected terrestrial mass points in month k. The element $dm_{j,k}$ in the solutions indicates the mass deviation at terrestrial mass point j in month k.

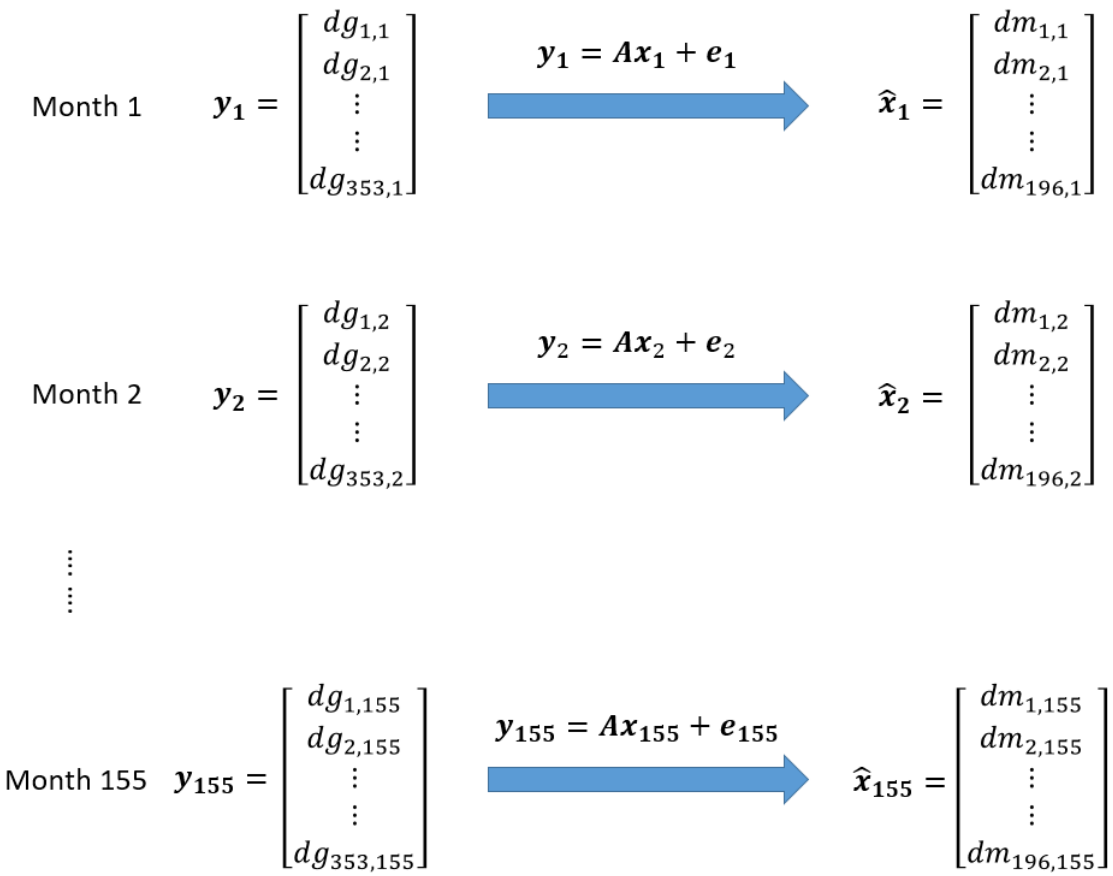

Figure 6.3: *The observation equations and the solutions containing monthly mass deviations*

According to the conclusion drawn in chapter 5, we know that when the distribution density of mass points is high and the observations is not noise-free, Tikhonov regularization is necessary to stabilize the least-squares solutions. So in our gravity inversion experiment, we need to apply L-curve criterion to find the proper regularization parameter like the simulation studies when solving these 155 observation equations. After plotting the solution norm against residual norm in the way of L-curve criterion for many observation equations, we find that the L-curves and also the parameters at the corner are very similar, which are always around 6.65×10^{-24}. For the sake of simplification, we determine this value as the proper regularization parameter for solving all the 155 observation equations and obtaining the respective Tikhonov-regularized least-squares solutions. Figure 6.4 is an example among these similar L-curves and optimal regularization parameters, which indicates the L-curve of the gravity inversion process in May 2004.

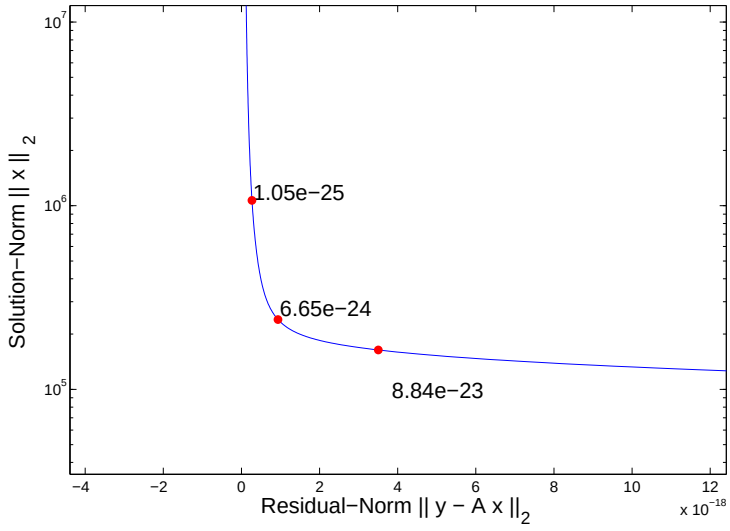

Figure 6.4: *The L-curve of the gravity inversion process, exemplary for the month May 2004*

6.3 The gravity inversion result

After conducting the gravity inversion process and solving the observation equations with Tikhonov regularization for each month, we can obtain 155 Tikhonov-regularized least-squares solutions for all the months, which are just the vectors containing the monthly mass deviations at those 196 selected terrestrial mass points over the Greenland area. Each element in one solution vector indicates the mass deviation of the corresponding mass point on the Earth's surface in the month represented by this solution vector. The sum of all the elements in one solution vector is the total mass deviation in the corresponding month. If we calculate the sum of each solution vector and plot them to the time series, we can derive the trend of the total mass change in Greenland in the 14-year time sequence. From this we can also apply linear regression to the time series to derive the secular total mass change over the whole 14-year time sequence. The result of plotting the data and linear regression is displayed in Figure 6.5. The red solid line is the linear regression result and its slope is the average total mass change per month. The secular total mass change over the whole time sequence is indicated as δm, whose value is -3973.96 Gt. Dividing δm by 14 we can obtain the average total mass change per year and the value is -283.85 Gt.

After plotting the monthly sum of the mass deviations and applying the linear regression, we derive the average total mass change per year in the 14-year sequence over the whole Greenland area. Meanwhile, if we plot the monthly mass deviations at a specific terrestrial mass point instead of the monthly sum of the mass deviations at all the 196 selected terrestrial mass points, we can also derive the trend of mass change, the secular mass change and the average mass change per year at this specific terrestrial mass point in the 14-year sequence. Here we select two coastal points (P_9 and P_{184}) from the 196 terrestrial mass points as examples for demonstration. The positions of P_9 and P_{184} on Greenland are displayed in Figure 6.6.

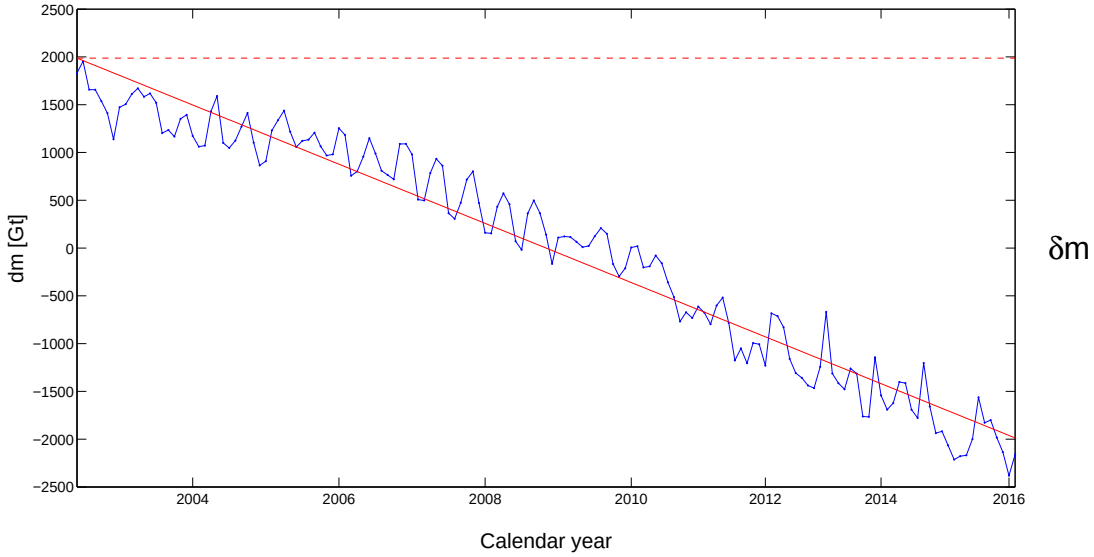

Figure 6.5: *The monthly total mass deviations and the linear regression result*

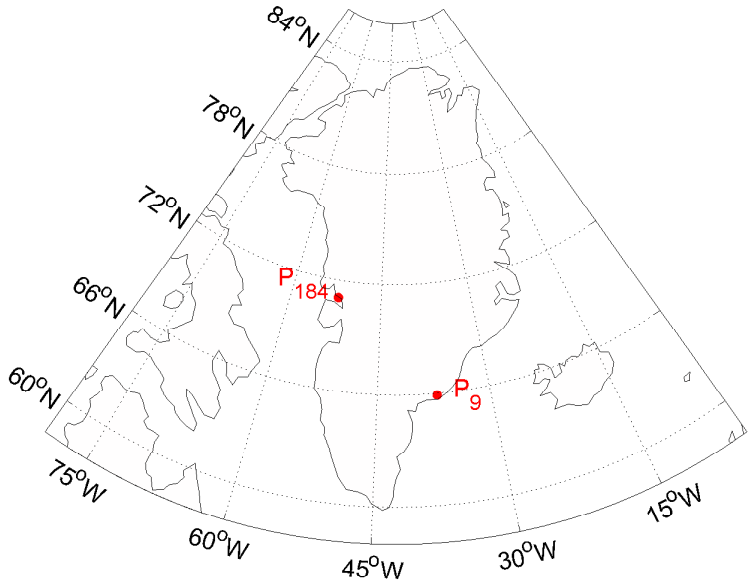

Figure 6.6: *The positions of terrestrial mass point P_9 and P_{184} on Greenland*

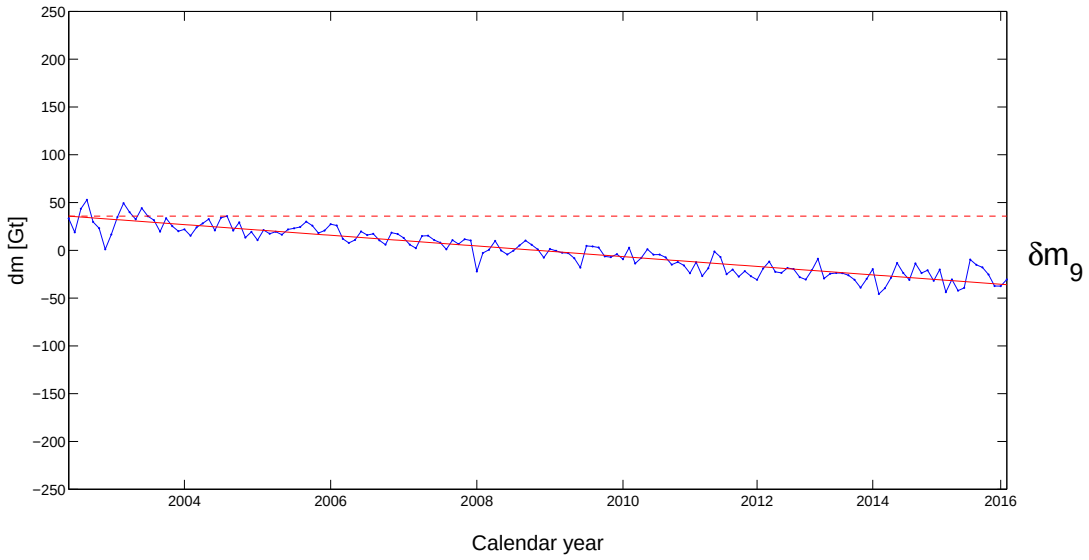

Figure 6.7: *The monthly mass deviations and the linear regression result at terrestrial mass point* P_9

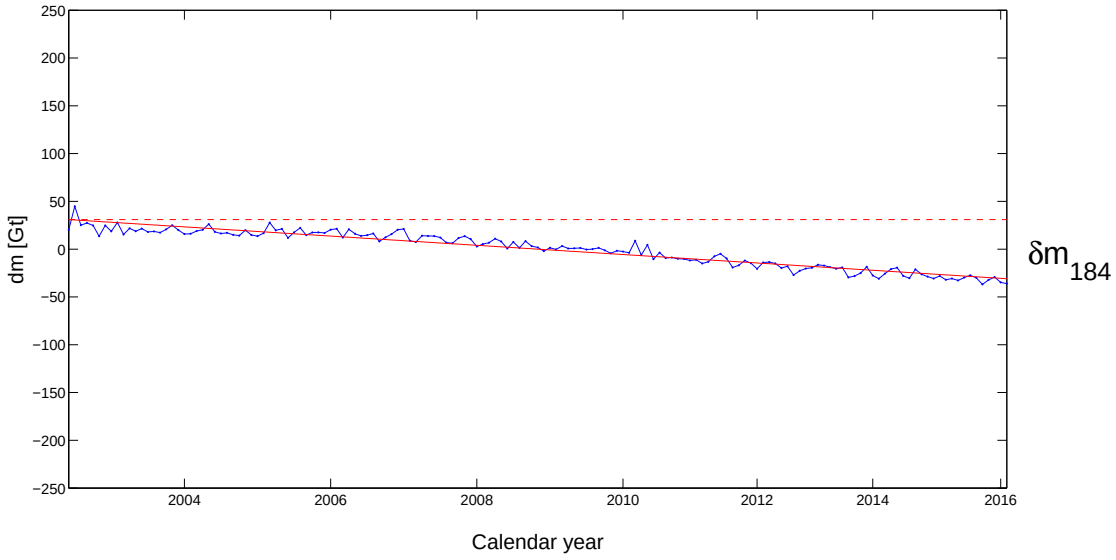

Figure 6.8: *The monthly mass deviations and the linear regression result at terrestrial mass point* P_{184}

Firstly we pick all the 9th elements $dm_{9,k}$ in each solution vector, which indicate the monthly mass deviations at P_9, and plot them to the time series. The indice k ($k = 1, 2, ..., 155$) represents the number of the month, i.e., the number of the solution vector. Then we also apply linear regression for the data to derive the secular mass change at P_9 over the whole time sequence, which is indicated as δm_9. The result of plotting the monthly mass deviations and the linear regression at P_9 is displayed in Figure 6.7. The red solid line is the linear regression result and its slope is the average mass change per month at terrestrial mass point P_9. Dividing δm_9 by 14 we can derive the average mass change per year at terrestrial mass point P_9 and the value is -5.12 Gt. Picking all the 184th elements $dm_{184,k}$ in each solution vector and performing the same steps for the terrestrial mass point P_{184}, we can derive the same information at P_{184}, which is shown in Figure 6.8, and the average mass change per year at P_{184} is -4.42 Gt.

P_9 and P_{184} are two examples among all the 196 selected terrestrial mass points. If we perform the same work at every single terrestrial mass point, we can derive the average mass change per year at all the 196 terrestrial mass points on Greenland. In other words, we respectively pick every single element with the same position from the solution vectors like the examples above, which indicates the monthly mass deviation at the corresponding terrestrial mass point in the month represented by the solution vector. Then we plot all the mass deviations from the 155 months to the time series at each terrestrial mass point and also apply linear regression for the data. From this we can derive the secular mass change over the whole time sequence and the average mass change pro year at all the 196 selected terrestrial mass points. Combining and visualizing the average mass change per year at all the mass points, we can acquire the information of mass loss distribution over the whole Greenland area, which is illustrated in Figure 6.9.

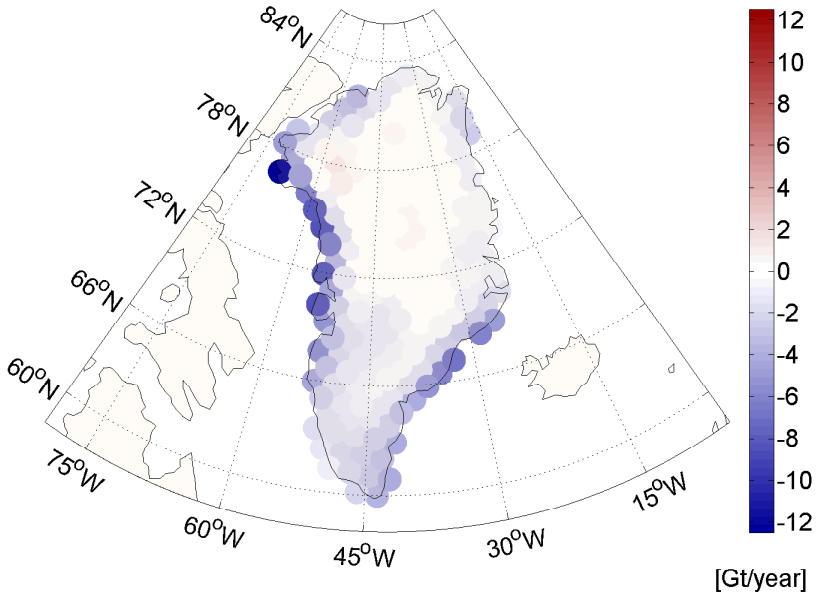

Figure 6.9: *The distribution of the mass variations on Greenland*

From Figure 6.9 we can find that the mass loss is mostly occurring on the border of Greenland, specially the west coast and the south-east coast regions. Inside Greenland the mass change is

not obvious and the magnitude is relatively small compared with that of the mass loss on the border. The magnitude of the average mass change per year at the selected 196 mass points on Greenland ranges from -12.38 Gt to 1.50 Gt. The maximal average mass loss per year (-12.38 Gt) occurs at the terrestrial mass point P_{55} and the maximal mass increase per year (1.50 Gt) occurs at the terrestrial mass point P_{59}. The positions of P_{55} and P_{59} are displayed in Figure 6.10.

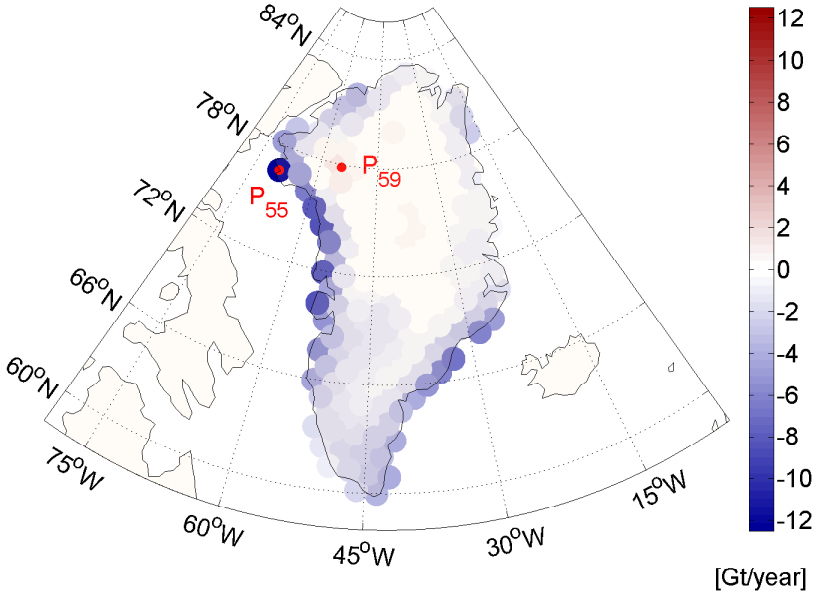

Figure 6.10: *The positions of terrestrial mass point P_{55} and P_{59} on Greenland*

Chapter 7

Conclusion

This work estimates the ice mass loss in Greenland in the 14-year time sequence from April 2002 to March 2016. The result shows us that in the investigated 14-year sequence Greenland loses on average around 283.85 Gt of ice every year, which means that near 300 km^3 of ice melts and flows into the ocean from Greenland every year. The ice mass loss mostly occurs on the border of Greenland, specially the west and south-east coastal regions. Inside Greenland the mass reduces or increases, but not significant compared with the loss in coastal regions. From the simulation studies and the real data experiment in this work we find that point-mass modelling can relate the gravitational signals at satellite altitude and the mass variations attributed to individual terrestrial points on the Earth's surface, which enables us to build up the geometrical relationship between both sides and yield the observation equations for the gravity inversion. In order to solve the observation equations, we need to apply Tikhonov regularization for the least-squares adjustment since in our studies the observations are not noise-free and the distribution density of mass points is high for high-resolution spatial mass variation patterns. The purpose of Tikhonov regularization is to stabilize the least-squares solution with a proper regularization parameter. The method used in this work to appropriately choose the optimal regularization parameter is L-curve criterion and it turns out to be an efficient method for this purpose in this work.

However, we still find some problems when applying the L-curve criterion to search the proper regularization parameter. The graph plotting the solution norm against residual norm is not always a typically L-shaped curve and sometimes the corner of the curve is very smooth, which makes the determination of the corner, i.e., the proper regularization parameter rather difficult. It causes that in some cases our choice of the parameter is possibly not the optimal. Another problem is that the L-curve criterion is based on a set of pre-defined parameters; then we calculate and plot the solution norm against residual norm respectively corresponding to the parameters. So it partly depends on the choice of the pre-defined parameters whether we can obtain the desired L-shaped graph with the corner.

Compared with the results of other studies we find that our estimation of the ice mass loss in Greenland in this work is reliable. The gravity inversion by means of point-mass modelling is a viable methodology to estimate the mass variations in a big area on the Earth's surface and it can also provides high-resolution spatial mass variation patterns when the distribution density of the terrestrial mass points is high enough in the studied area on the Earth's surface. Hence, we can also apply this efficient methodology to derive rational estimations of the mass change in other regions on the Earth's surface.

Bibliography

Baur, O. and Sneeuw, N. Assessing Greenland ice mass loss by means of point-mass modeling: a viable methodology. *Journal of Geodesy*, 85:607–615, 2011. doi: 10.1007/s00190-011-0463-1.

Chen, T., Shen, Y., and Chen, Q. Mass flux solution in the Tibetan plateau using mascon modeling. *remote sensing*, 8:439, 2016. doi: 10.3390/rs8050439.

Google. Google earth, software, google inc. `https://www.google.com/earth/`, 2017. Accessed on June 10, 2017.

Hansen, P.C. Regularization tools. `http://www.imm.dtu.dk/pcha/Regutools/`, 2008. Accessed on June 10, 2017.

Hurt, P. Untersuchung von Schweredifferenzen durch Punktmassenmodellierung anhand der GRACE-Schwerefelddaten eines Gletschergebietes. `https://elib.uni-stuttgart.de/handle/11682/4000`, 2015. Accessed on June 10, 2017.

NASA. Mission overview. `https://www.nasa.gov/`, 2012. Accessed on June 10, 2017.